

Warming early Mars with CO₂ and H₂

Ramses M. Ramirez^{i,iii,v}, Ravi Kopparapu^{i,iii,v}, Michael E. Zugger^{ii,v}, Tyler D. Robinson^{iv,v},
Richard Freedman^{vi}, and James F. Kasting^{i,iii,v}

ⁱ Department of Geosciences, ⁱⁱ Applied Research Laboratory, ⁱⁱⁱ Penn State Astrobiology
Research Center, Penn State University University Park, PA 16802

^{iv} Astronomy Department. University of Washington, Box 351580, Seattle, WA 98195

^v NASA Astrobiology Institute Virtual Planetary Laboratory

^{vi} SETI Institute, Mountain View, CA 94043/NASA Ames Research Center, Moffett Field, CA,
94035

Abstract

The presence of valleys on ancient terrains of Mars suggest that liquid water flowed on the martian surface 3.8 billion years ago or before. The above-freezing temperatures required to explain valley formation could have been transient, in response to frequent large meteorite impacts on early Mars, or they could have been caused by long-lived greenhouse warming. Climate models that consider only the greenhouse gases carbon dioxide and water vapor have been unable to recreate warm surface conditions, given the lower solar luminosity at that time. Here we use a one-dimensional climate model to demonstrate that an atmosphere containing 1.3-4 bar of CO₂ and water vapor, along with 5-20 percent H₂, could have raised the mean surface temperature of early Mars above the freezing point of water. Vigorous volcanic outgassing from a highly reduced early martian mantle is expected to provide sufficient atmospheric H₂ and CO₂ - the latter from the photochemical oxidation of outgassed CH₄ and CO - to form a CO₂-H₂ greenhouse. Such a dense early martian atmosphere is consistent with independent estimates of surface pressure based on cratering data.

The climate of early Mars has been a topic of debate for at least the last 30 years. Nearly all researchers agree that the martian valleys and valley networks were formed by running water¹. Debate has persisted as to how warm the surface must have been to form these features and how long this warmth must have lasted². The widely cited impact hypothesis³⁻⁵ suggests that large impacts occurring during the Heavy Bombardment Period could have heated the surface for brief intervals and that the valleys were formed by water that rained out following these events. Other authors⁶ have argued that the martian climate was warmed by the greenhouse effect of a dense CO₂-H₂O atmosphere, perhaps supplemented with SO₂⁷. But the SO₂ warming mechanism has difficulties because of photochemical production of sulfate aerosols, which act to cool the climate⁸, and the calculation in ref. 7 is no longer believed because of errors in the CO₂ absorption coefficients⁹. Furthermore, all recent one-dimensional CO₂-H₂O climate models^{8,10,11} have been unable to produce above-freezing surface temperatures because of a combination of two factors: 1) CO₂ condensation, which reduces the tropospheric lapse rate, thereby lowering the greenhouse effect, and 2) Rayleigh scattering, which causes the planet's albedo to become high as the surface pressure becomes large¹⁰. Forget and Pierrehumbert¹² were able to produce mean surface temperatures above the freezing point of water by including explicit CO₂ ice clouds with 100 percent cloud cover. However, 3-D climate models predict much smaller fractional CO₂ cloud cover and greatly reduced surface warming.^{13,14}

An updated 1-D climate calculation illustrates the basic problem (see Fig. 1). When solar luminosity is >80 percent of today's value, increased CO₂ partial pressure is capable of bringing Mars' mean surface temperature above 273 K. But for solar luminosities ≤80 percent of today, corresponding to time periods prior to ~2.8 Gyr ago¹⁵, no amount of CO₂ can produce a warm surface. Instead, a dense CO₂ atmosphere would simply condense out globally in a 1-D climate

model or at the poles in a more realistic 3-D climate model¹⁴. The perceived difficulty in producing a stable, warm climate on early Mars has bolstered support for the impact hypothesis, along with other “cold early Mars” theories.

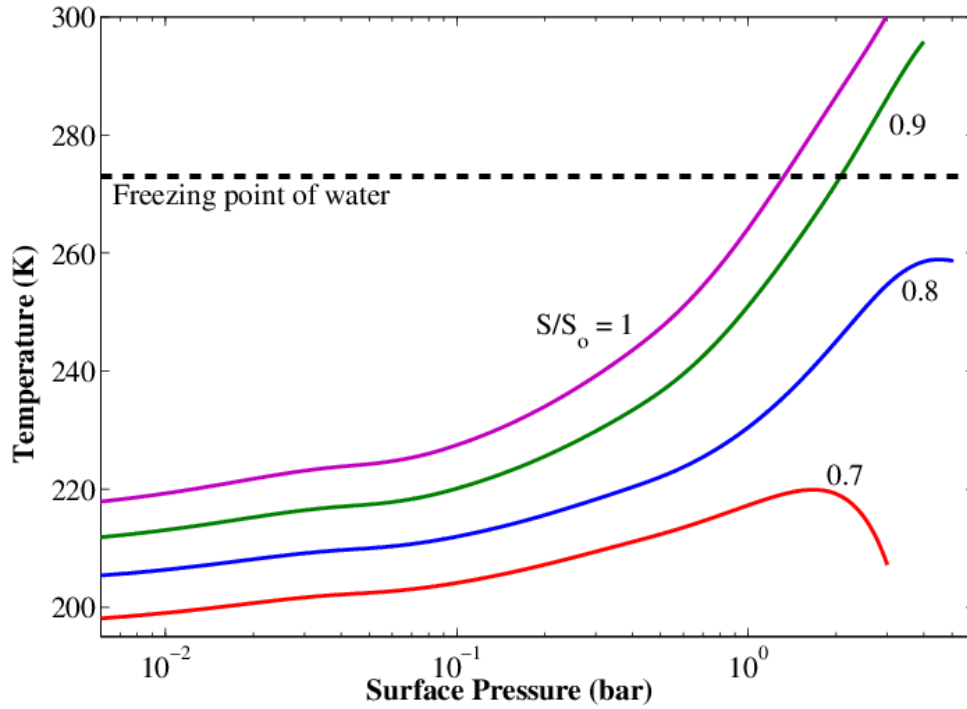


Fig. 1: Mean surface temperature as a function of surface pressure for a fully saturated (95% CO₂, 5% N₂) early Mars atmosphere at different solar insolation levels. The assumed surface albedo is 0.216. These results agree to within a few degrees with those of ref. (8), largely because increased absorption in the far wings of CO₂ and H₂O lines (see Supp. Info) compensated for the loss of absorption arising from the updated CO₂ CIA parametrization (from ref. 11).

Since the impact hypothesis was proposed, other workers have pointed out that the valleys are more extensive than originally realized¹⁶, and some have argued that the amount of

time and surface runoff needed to form them was much larger than had been previously assumed^{17,18}. Hoke et al.¹⁸ performed detailed hydrologic modeling of several different valleys listed in their Table 3. The larger ones (*e.g.*, the 2°N, 34°E Naktong east valley) require episodic runoff rates of 0.5 cm/day, along with intermittent runoff averaging ~10 cm/yr for $(3-4) \times 10^7$ yr. These high flow rates are needed to lift eroded material off the river bed and keep it in suspension. According to Hoke et al., the estimated runoff total for this one valley is 3-4 million meters, or more than three orders of magnitude more than the amount of rainwater provided by the impact hypothesis. So, these authors envision an entirely different, and much wetter, scenario for martian valley formation. Here, we propose a mechanism for supplying these significantly larger rainfall amounts.

Greenhouse warming by models that include H₂

The utility of H₂ as a greenhouse gas for terrestrial planets was pointed out several years ago by Stevenson¹⁹ and has been studied more quantitatively by recent authors.^{20,21} Wordsworth and Pierrehumbert²¹ showed that early Earth could have been kept warm by greenhouse warming from collision-induced absorption (CIA) caused by the interaction of H₂ molecules with N₂. These collisions excite the pure rotational levels of H₂ and, at the same time, allow it to absorb electromagnetic radiation to lift it from one rotational state to the next. At room temperature, the absorption spectrum of H₂ extends right through the 8-12 μm “window region”, allowing it to be an effective greenhouse gas on either early Earth or Mars.^{21,22} One difference between the two planets is that Mars has long been deficient in N₂²³, and so the main broadening gas there may instead have been CO₂. Collisional excitation of H₂ by CO₂ has not been studied, but there is no reason to suppose that it would be any less efficient than excitation by N₂. Indeed, collisional

broadening of permitted absorption lines is stronger for CO₂ (Supp. Info.). Below, we conservatively assume that H₂-CO₂ CIA is of the same strength as H₂-N₂ CIA, for which the excitation cross sections have been calculated theoretically²⁴.

We included H₂ CIA, along with other updates, in our existing 1-D radiative-convective climate model²⁵. Details are provided in Supp. Info. We then performed a series of climate calculations for hypothetical martian paleoatmospheres containing various amounts of CO₂ and H₂ (Fig. 2). The assumed solar luminosity was 0.75 times present, which is appropriate for 3.8 Gyr ago¹⁵. When H₂ was absent, the mean surface temperature never exceeded 230 K, regardless of how much CO₂ was present. This temperature is similar to values found previously by our group: published maximum temperatures for this solar flux were ~225 K¹⁰ and 231 K⁸. Wordsworth et al.¹¹ could reach only 217 K for a 1-bar CO₂ atmosphere, but their model did not include H₂O.

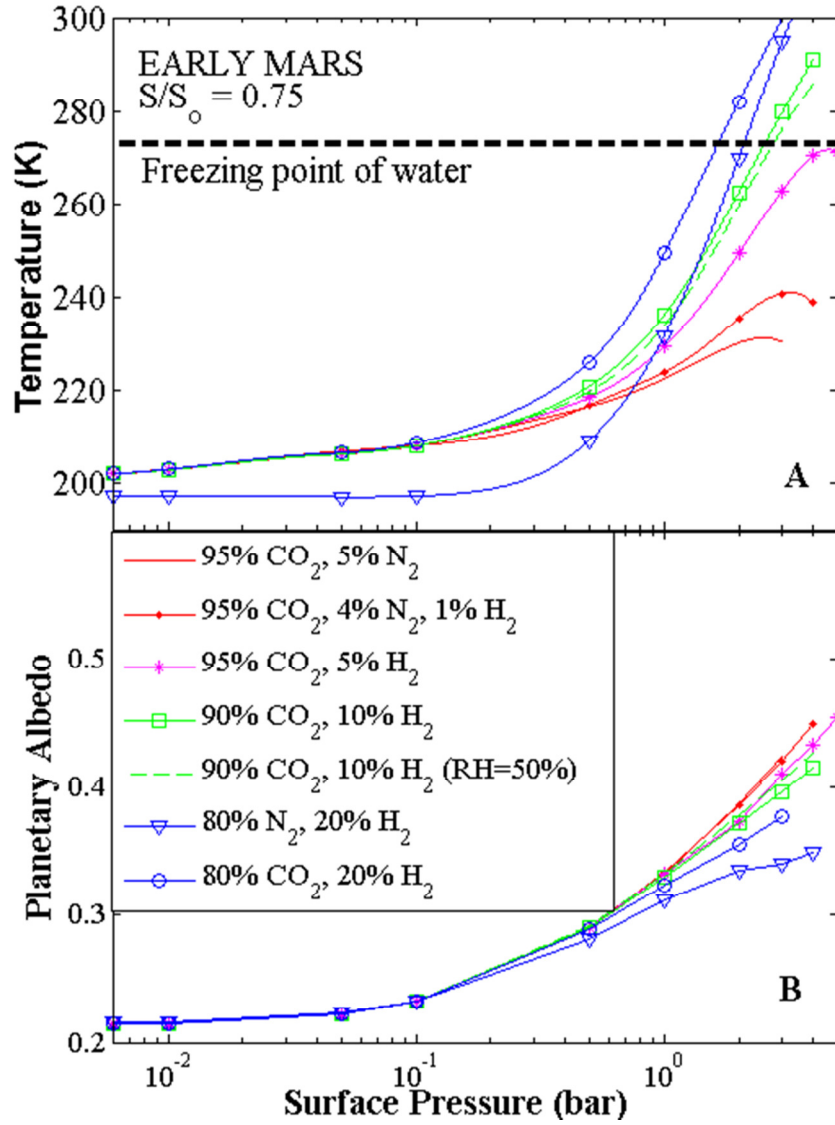


Fig. 2: Surface temperature (a) and planetary albedo (b) as a function of surface pressure for different atmospheric compositions. The assumed solar luminosity is 0.75 times present, appropriate for 3.8 Gyr ago. Any remaining gas not accounted for in the legend is considered to be N_2 . Solid curves correspond to fully saturated atmospheres, while the model represented by the dashed curve assumes 50% tropospheric relative humidity. At 273 K and 10% H_2 , a difference of only ~3-4 K separates the fully saturated and 50% relative humidity cases, indicating that the vast majority of the greenhouse warming is caused by H_2 - CO_2 collision-induced absorption.

When 5 percent H_2 was included in our new climate model, the calculated maximum surface temperature nearly reached 273 K as CO_2 was increased, and it exceeded 273 K when the solar radiation calculation was done more accurately (Supp. Info.). The corresponding surface pressure for this simulation was ~4 bar (or ~3 bar in the more accurate calculation). Warming by CO_2 ice clouds^{12,14}, or H_2O cirrus clouds²⁶, both of which were neglected in these calculations, would increase the mean surface temperature still further; thus, we take 5 percent as a reasonable minimum estimate for the H_2 concentration needed to produce a mean surface temperature above freezing. Higher H_2 concentrations allow the freezing point to be reached at lower surface pressures. For 10 percent H_2 this threshold was reached at ~2.5 bar, and for 20 percent H_2 it was reached at ~1.6 bar. This latter value is below the upper limit of 1.9 bar calculated recently by Kite et al.²⁷ based on the size distribution of secondary craters from impacts. Those calculations assume a weak soil target strength consistent with river alluvium; for a harder bedrock surface the upper limit on pressure approximately doubles²⁷. H_2 - N_2 collisions could also conceivably have warmed Mars to this temperature for N_2 partial pressures >2 bar, although N_2 is less likely to have been present in abundance, as already noted.

Finally, we acknowledge that the goal of reaching a mean surface temperature of 273 K may be somewhat artificial, as both temperatures and precipitation rates vary as a function of latitude and altitude. Wolf and Toon²⁸ used a 3-D climate model to show that half of Earth's early oceans could have remained unfrozen at a mean temperature of only 260 K, and the same could be true for early Mars^{13,26}. So, more realistic climate simulations may show that the valleys could have formed at somewhat lower concentrations of H_2 and/or CO_2 .

Sources and sinks for H₂ and CO₂

Both H₂ and CO₂ would have to have been abundant on early Mars for this greenhouse warming mechanism to have succeeded. We assume that early Mars, like early Earth, was volcanically active and would have released H, C, and S-bearing gases. We begin our analysis by considering outgassing of hydrogen on modern Earth. On Earth, the dominant outgassed form of H for subaerial volcanism is H₂O²⁹, which has an outgassing rate of 1.0×10^{14} mol yr⁻¹ (ref. 30). The H₂:H₂O ratio in subaerial volcanic gases can be estimated by considering thermodynamic equilibrium at typical outgassing conditions (1450 K, 5 bar pressure)²⁹ for the following reaction



The H₂:H₂O ratio, R , is given by the relation

$$\frac{p\text{H}_2}{p\text{H}_2\text{O}} \equiv R = \left(\frac{K_1}{f\text{O}_2} \right)^{0.5} \quad (2)$$

Here, $p\text{H}_2$ and $p\text{H}_2\text{O}$ are the partial pressures of H₂ and H₂O in the released gas, and $f\text{O}_2$ is the oxygen fugacity of the system, which is set by the magma. The equilibrium constant, K_1 , calculated from Gibbs free energies (see Supp. Info.), is 1.80×10^{-12} atm. For the relatively oxidized Earth, the oxygen fugacity is near the QFM (quartz-fayalite-magnetite) synthetic buffer, for which $f\text{O}_2 \cong 10^{-8.5}$ at these P-T conditions³¹, and so the predicted H₂:H₂O ratio is 0.024.

Multiplying by the outgassing rate for H₂O gives a subaerial H₂ outgassing flux of 2.4×10^{12} mol/yr, or 1×10^{10} H₂ molec cm⁻² s⁻¹. (The actual H₂ outgassing rate scales as $R/(1+R)$, as can be demonstrated from mass balance, but this ratio reduces to R when $R \ll 1$.) This value is essentially identical with the estimate of total H₂ outgassing by Holland³². About half of Holland's total H₂ flux comes from submarine H₂S, which is readily photolyzed⁸, and which can

be converted to H₂ equivalents by the reaction: $\text{H}_2\text{S} + 2 \text{H}_2\text{O} \rightarrow \text{SO}_2 + 3 \text{H}_2$. (Further discussion of the atmospheric redox budget is given in Supp. Info.) Our calculated subaerial H₂ flux may thus be too high by a factor of 2, but by making this error we implicitly account for the contribution from H₂S. Scaling the outgassing rate in this manner might actually underestimate the H₂S flux, considering that Mars' mantle appears to be exceptionally rich in sulfur³³. The H₂ outgassing rate for modern Earth is uncertain by at least a factor of 5 (ref. 32), so trying to refine our estimate further would have limited benefit.

How might these outgassing fluxes scale for early Mars? It is difficult to be certain, partly because we do not know whether Mars ever experienced plate tectonics. We can make some crude analogies, however. The geothermal heat flux on Mars during the Noachian era is thought to have been similar to that of modern Earth³⁴, so it is plausible to assume that the total (H₂O+H₂) outgassing rate per unit area was the same on the two planets. The H₂ mole fraction should have been higher on Mars, though, because Mars' mantle is thought to be more reduced. Martian meteorites (SNCs) have $f\text{O}_2$'s ranging from QFM down to IW (iron-wüstite) or below^{35,36}. (The IW O₂ buffer is about 4 log units below QFM.) The shergottites, which are the most primitive SNCs petrologically, and hence most like the mantle, have $f\text{O}_2$ values of ~IW+1³⁶. And ALH84001, the oldest martian meteorite, is at IW–1, suggesting that the early martian mantle may have been even more reduced³⁶. This prediction is in conflict with a recent analysis based on S and Ni abundances and the Mn/Fe ratio of Gusev crater rocks, which suggest that the upper part of Mars' early mantle was more oxidized in the distant past³⁷. But these data might also be explained by later alteration³⁷, so the bulk of the evidence still favors a highly reduced early mantle.

Assume for the moment that Mars' mantle fO_2 was near IW+1, roughly 3 log units below the terrestrial value. Eq. (2) then predicts that the $H_2:H_2O$ ratio, R , in the released gas should increase by a factor of 32. The rate of H_2 outgassing should increase by a smaller amount ($\propto R/(1+R)$), assuming that the total outgassing rate of (H_2+H_2O) remains constant. . The three-log-unit decrease in mantle fO_2 compared to Earth should increase H_2 outgassing by a factor of ~ 20 , so the expected H_2 outgassing rate on early Mars should be of the order of $(1 \times 10^{10} \text{ cm}^{-2} \text{ s}^{-1}) \times 20 = 2 \times 10^{11} \text{ cm}^{-2} \text{ s}^{-1}$. This direct flux of H_2 could have been augmented by $\sim 50\%$ by an indirect flux of hydrogen from CH_4 (see below and Supp. Info.), but we neglect that contribution here. This input of hydrogen should have been balanced by escape of hydrogen to space. If hydrogen escaped at the diffusion limit³⁸, the escape rate in these same units would be given by

$$\Phi_l(H_2) = \frac{b_i}{H_a} \cdot \frac{f_T(H_2)}{1 + f_T(H_2)} \cong \frac{b_i f_T(H_2)}{H_a} \quad (2)$$

Here, b_i is a weighted molecular diffusion coefficient for H and H_2 in air (or CO_2), H_a ($= kT / mg$) is the pressure scale height, and $f_T(H_2)$ is the total hydrogen volume mixing ratio: $f_T(H_2) = 0.5f(H) + f(H_2) + f(H_2O) + \dots$. If H_2 is the dominant H-bearing species, then $f_T(H_2) \cong f(H_2)$. All quantities are evaluated at the homopause, near 130 km altitude on present Mars, where molecular diffusion begins to exceed mixing by turbulent eddies. Counter-intuitively, Mars' lower gravity *decreases* the hydrogen escape rate compared to Earth because the scale height, H_a , appears in the denominator of eq. (2). For a homopause temperature of ~ 160 K, $b_i/H_a \cong 1.6 \times 10^{13} \text{ cm}^{-2} \text{ s}^{-1}$. Inserting this value into eq. (2) and equating H_2 escape with H_2 outgassing yields $f(H_2) \cong 0.013$. This is a factor of 4 less than the minimum H_2 mixing ratio of 0.05 needed to produce Earth-like surface temperatures on early Mars, according to Fig. 2. At a mantle fO_2 of IW-1, the H_2 outgassing flux would be another factor of 2 higher, making it

$4 \times 10^{11} \text{ cm}^{-2} \text{ s}^{-1}$ and yielding an atmospheric H_2 mixing ratio of ~ 0.025 , about half the minimum H_2 concentration needed to produce a warm early Mars (Fig. 2).

These numbers are all very uncertain, though. Volcanic outgassing rates on early Mars could have been considerably higher than those on modern Earth, and/or hydrogen may have escaped at less than the diffusion-limited rate. Calculations with our own 1-D hydrodynamic escape model, which is based on that of ref. 39, suggest that the diffusion limit would have been achieved. However, such 1-D calculations may overestimate the actual escape rate. The escape geometry is at least 2-dimensional, as solar radiation impinges on only one side of the planet. A third dimension is required if magnetic fields are included and if the planet's magnetic axis is inclined relative to its orbital plane. For neutral, nearly isothermal atmospheres escaping from hot Jupiter exoplanets, geometry alone reduces the mass loss rate by nearly a factor of 4 (ref. 40). That would bring the predicted atmospheric H_2 mixing ratio in our model up to 10 percent if Mars' mantle was at IW-1, or 5 percent at IW+1. Accounting for partial ionization of the escaping gases and their interaction with a planetary magnetic field, which might have existed up until $\sim 3.9\text{-}4.0 \text{ Ga}^{41}$, might slow the escape even further, so H_2 mixing ratios of 20 percent are not impossible. More complicated magnetohydrodynamic escape models would be needed to study this possibility.

Availability of CO_2 must also be considered. On Earth, the atmospheric CO_2 abundance is controlled over long time scales by the balance between production by volcanism and loss by weathering of silicate minerals followed by precipitation of carbonates. CO_2 is predicted to accumulate in the atmosphere when the climate is cold because of slower weathering⁴², and this feedback process could have been important on early Mars, as well⁶. On Mars, however, the total carbon inventory is uncertain, and additional terms in the CO_2 budget must be considered.

Carbonate minerals are observed in martian dust and in the SNC meteorites^{43,44}. If the carbonate content of the dust is representative of the uppermost 2 km of crust, then the crust could contain the equivalent of 5 bar of CO₂⁴⁴. This inference is speculative, however, and the apparent lack of large carbonate outcrops in the martian subsurface⁴³ suggests that much of Mars' CO₂ was lost by escape to space. CO₂ can be lost by both thermal⁴⁵ and nonthermal⁴⁶ loss processes. Thermal escape, which might initially have been very fast, presents the greatest hurdle for maintaining a dense early martian atmosphere. Thermal (hydrodynamic) loss of both C and O is predicted when the solar extreme ultraviolet (EUV) flux is more than ~5 times the modern solar mean, which would likely have been the case during the first several hundred million years of Mars' history⁴⁷. Modeling suggests that the best time to accumulate CO₂ would be 3.8-4.0 Gyr ago, when solar activity had declined but when volcanoes were still active⁴⁵.

A second concern is whether enough CO₂ would have been supplied from volcanoes to maintain a dense atmosphere. Phillips et al.⁴⁸ estimated that 1.5 bar of CO₂ would have been emitted by Tharsis alone. But, because of Mars' much lower mantle oxygen fugacity, some authors have suggested that most of Mars' carbon would have been retained in the mantle as graphite^{35,36}. These studies estimate upper limits of ~1 bar on outgassed CO₂ if Mars' mantle f_{O_2} was near IW+1. Just recently, however, Wetzel et al.⁴⁹ have studied this system experimentally and have shown that carbon would be stored in reduced silicate melts as a mixture of iron carbonyl, Fe(CO)₅, and CH₄. Upon outgassing, iron carbonyl would dissociate to form CO. According to their estimates, initial solidification of a 50 km-thick crust would have released 1 bar of CO and 1.3 bar of CH₄. Once in the atmosphere, both of these gases would have been oxidized by the byproducts of water vapor photolysis²⁵, yielding ~5.2 bar of CO₂ as an initial atmospheric inventory. CO₂ would have been continuously removed by carbonate formation and

by escape, so recycling and/or continued juvenile outgassing would have been needed to maintain its abundance. To complicate matters, CO might have been more abundant than CO₂ if the carbon was outgassed in reduced form⁵⁰. Although CO is not an effective greenhouse gas, calculations with N₂-H₂ mixtures (Fig. 2a) show that the surface can still be warmed above the freezing point even if the accompanying gas is not radiatively active. CH₄ is an effective greenhouse gas on modern Earth; however, our calculations indicate that its contribution to Mars' greenhouse effect was negligible (see Supp. Info.).

In summary, the formation of valleys and valley networks on early Mars is most easily explained if the climate was warm for long time periods. An H₂-CO₂-H₂O greenhouse is capable of sustaining mean surface temperatures > 0°C at 3.8 Gyr ago, provided that H₂ and CO₂ were maintained at reasonably high concentrations (5 percent for H₂, >1.3 bar for CO₂) by volcanic outgassing. CO also works in combination with H₂ at slightly higher surface pressures. High concentrations of H₂ would have been promoted by outgassing from a strongly reduced martian mantle, perhaps augmented by geometric or magnetic limitations on the rate at which H₂ escaped to space. CO₂ could have been supplied either directly if the mantle was relatively oxidized or indirectly as CO and CH₄ if the mantle was highly reduced. More detailed exploration of Mars' surface, including searches for buried carbonates, could provide additional evidence to test this hypothesis.

Methods Summary

The climate calculations described here were performed with a 1-dimensional (horizontally averaged) global climate model. Details and references are provided in Supp. Info. In such a model, the planet is assumed to be flat, and the Sun is placed at a solar zenith angle of 60° from the vertical. Because $\cos(60^\circ) = 0.5$, multiplying the resulting solar fluxes by another

factor of 0.5 gives the planetary average mean solar flux of $S/4$, where S is the solar constant at the planet's orbit. Some sensitivity tests were performed with a more accurate, Gaussian integration over solar zenith angles (see Supp. Info.). In both the solar and thermal-infrared parts of the radiation code, the diffuse flux was calculated using a 2-stream approximation in which the integration over the upward and downward hemispheres is accomplished by choosing a single average zenith angle. In such a model, the stratosphere is assumed to be in radiative equilibrium, that is, the net emitted infrared flux is equal to the net absorbed solar flux in each layer. In the troposphere (nearer to the planet's surface), convection was accounted for by using a moist convective adjustment, as follows: If the temperature lapse rate calculated from radiative equilibrium exceeded the moist adiabatic lapse, the lapse rate in that layer was adjusted back to the moist adiabat. Here, the term "moist" refers to saturation with either H_2O or CO_2 . Typically, H_2O condenses within the lower part of the planet's troposphere, whereas CO_2 condenses in the upper troposphere. As described in the main text, the troposphere was assumed to be fully saturated with H_2O in most of our simulations. This produces a slight overestimate for the surface temperature, but the error should be generally small (see Fig. 2). More importantly, the effect of clouds on the planetary albedo is not calculated accurately in our model; instead, the atmosphere is assumed to be cloud-free, and the surface albedo is adjusted to a value (0.216) that allows the model to reproduce Mars' current mean surface temperature, 218 K, given current solar insolation. This surface albedo is held fixed for all the calculations shown in Figs. 1 and 2. More complex, 3-D climate models are needed to treat clouds and relative humidity more realistically.

References

1. Carr, M. H. The martian drainage system and the origin of valley networks and fretted channels. *J. Geophys. Res.* **100**, 7479-7507 (1995).
2. Jakosky, B. M., Haberle, R. M. & Arvidson, R. E. The changing picture of volatiles and climate on Mars. *Science* **310**, 1439-1440 (2005).
3. Segura, T. L., Toon, O. B., Colaprete, A. & Zahnle, K. Environmental effects of large impacts on Mars. *Science* **298**, 1977-1980 (2002).
4. Segura, T. L., Toon, O. B. & Colaprete, A. Modeling the environmental effects of moderate-sized impacts on Mars. *Journal of Geophysical Research-Planets* **113** (2008).
5. Segura, T. L., McKay, C. P. & Toon, O. B. An impact-induced, stable, runaway climate on Mars. *Icarus* **220**, 144-148 (2012).
6. Pollack, J. B., Kasting, J. F., Richardson, S. M. & Poliakov, K. The case for a wet, warm climate on early Mars. *Icarus* **71**, 203-224 (1987).
7. Johnson, S. S., Mischna, M. A., Grove, T. L. & Zuber, M. T. Sulfur-induced greenhouse warming on early Mars. *Journal of Geophysical Research-Planets* **113** (2008).
8. Tian, F. *et al.* Photochemical and climate consequences of sulfur outgassing on early Mars. *Earth and Planetary Science Letters* **295**, 412-418 (2010).
9. Mischna, M., Baker, V., Milliken, R., Richardson, M., Lee, C. Effects of obliquity and water vapor/trace gas greenhouses in the early Martian climate. *J. Geophys. Res.*, **118**, 1-17 (2013).
10. Kasting, J. F. CO₂ condensation and the climate of early Mars. *Icarus* **94**, 1-13 (1991).
11. Wordsworth, R., Forget, F. & Eymet, V. Infrared collision-induced and far-line absorption in dense CO₂ atmospheres. *Icarus* **210**, 992-997 (2010).

12. Forget, F. & Pierrehumbert, R. T. Warming early Mars with carbon dioxide clouds that scatter infrared radiation. *Science* **278**, 1273-1276 (1997).
13. Wordsworth R., Forget, F., Millour, E., Head, J. W., Madeleine, J.-B., Charnay, B. Global modelling of the early Martian climate under a denser CO₂ atmosphere: Water cycle and ice evolution. *Icarus* **222**, 1-19 (2013).
14. Forget, F. *et al.* 3D modelling of the early martian climate under a denser CO₂ atmosphere: Temperatures and CO₂ ice clouds. *Icarus* **222**, 81-99 (2013).
15. Gough, D. O. Solar interior structure and luminosity variations. *Solar Phys.* **74**, 21-34 (1981).
16. Hynek, B. M. & Phillips, R. J. New data reveal mature, integrated drainage systems on Mars indicative of past precipitation. *Geology* **31**, 757-760 (2003).
17. Barnhart, C. J., Howard, A. D. & Moore, J. M. Long-term precipitation and late-stage valley network formation: Landform simulations of Parana Basin, Mars. *Journal of Geophysical Research-Planets* **114** (2009).
18. Hoke, M. R. T., Hynek, B. M. & Tucker, G. E. Formation timescales of large Martian valley networks. *Earth and Planetary Science Letters* **312**, 1-12 (2011).
19. Stevenson, D. J. Life-sustaining planets in interstellar space? *Nature* **400**, 32-32 (1999).
20. Pierrehumbert R. & Gaidos E. Hydrogen greenhouse planets beyond the habitable zone. *Astrophysical Journal Letters*. 734(1) (2011).
21. Wordsworth, R. & Pierrehumbert, R. Hydrogen-nitrogen greenhouse warming in Earth's early atmosphere. *Science* **339**, 64-67 (2013).
22. Kasting, J. F. How was early Earth kept warm? *Science* **339**, 44-45 (2013).
23. Fox, J. L. The production and escape of nitrogen atoms on Mars. *J. Geophys. Res.* **98**, 3297-3310 (1993).

24. Borysow, A. & Frommhold, L. Theoretical collision-induced rototranslational absorption-spectra for modeling titans atmosphere - H₂-N₂ pairs. *Astrophysical Journal* **303**, 495-510 (1986).
25. Haqq-Misra, J. D., Domagal-Goldman, S. D., Kasting, P. J. & Kasting, J. F. A revised, hazy methane greenhouse for the early Earth. *Astrobiol.* **8**, 1127-1137 (2008).
26. Urata, R. A. & Toon, O. B. Simulations of the martian hydrologic cycle with a general circulation model: Implications for the ancient martian climate. *Icarus* **226**, 229-250 (2013).
27. Kite, E., Williams, J-P, Lucis, A., Aharonson, O. Low paleopressure of the martian atmosphere estimated from the size distribution of ancient craters. *Nat. Geosc.* **7**, 335-339 (2014).
28. Wolf, E. T. and Toon, O. B. Hospitable Archean climates simulated by a general circulation model *Astrobiology* **13**, 656-673 (2013).
29. Holland, H. D. *The Chemical Evolution of the Atmosphere and Oceans*, Table 2.6. (Princeton University Press, Princeton, 1984).
30. Jarrard, R. D. Subduction fluxes of water, carbon dioxide, chlorine, and potassium. *Geochemistry Geophysics Geosystems* **4** (2003).
31. Frost, B. R., in *Reviews in Mineralogy*, v. 25, *Oxide Minerals: Petrologic and Magmatic Significance* (D. H. Lindsley, ed., Mineral. Soc. Amer., BookCrafters, Inc., Chelsea, MI, pp. 1-9).
32. Holland, H. D. Why the atmosphere became oxygenated: A proposal. *Geochimica Et Cosmochimica Acta* **73**, 5241-5255 (2009).
33. Gaillard, F. & Scaillet, B. The sulfur content of volcanic gases on Mars. *Earth and Planetary*

- Science Letters* **279**, 34-43 (2009).
34. Montesi, L. G. J. & Zuber, M. T. Clues to the lithospheric structure of Mars from wrinkle ridge sets and localization instability. *Journal of Geophysical Research-Planets* **108** (2003).
35. Stanley, B. D., Hirschmann, M. M. & Withers, A. C. CO₂ solubility in Martian basalts and Martian atmospheric evolution. *Geochimica Et Cosmochimica Acta* **75**, 5987-6003 (2011).
36. Grott, M., Morschhauser, A., Breuer, D. & Hauber, E. Volcanic outgassing of CO₂ and H₂O on Mars. *Earth and Planetary Science Letters* **308**, 391-400 (2011).
37. Tuff, J., Wade, J., and Wood, B. J. Volcanism on Mars controlled by early oxidation of the upper mantle. *Nature* **498**, 342-345 (2013).
38. Walker, J. C. G. *Evolution of the Atmosphere*. (Macmillan, 1977).
39. Tian F., Kasting, J. F., Liu, H. L., and Roble, R. G. Hydrodynamic planetary thermosphere model: 1. Response of the Earth's thermosphere to extreme solar EUV conditions and the significance of adiabatic cooling. *Journal of Geophysical Research-Planets* **113** (2008).
40. Stone, J. M. & Proga, D. Anisotropic winds from close-in extrasolar planets. *Astrophysical Journal* **694**, 205-213 (2009).
41. Werner, The early martian evolution – Constraints from basin formation ages. *Icarus*, **195**, 45-60 (2008).
42. Walker, J. C. G., Hays, P. B. & Kasting, J. F. A negative feedback mechanism for the long-term stabilization of Earth's surface temperature. *J. Geophys. Res.* **86**, 9776-9782 (1981).
43. Bandfield, J. L., Glotch, T. D. and Christensen, P. R. *Science* **301**, 1084-1087 (2003).
44. Lammer, H. *et al.* Outgassing history and escape of the martian atmosphere and water

- inventory. *Space Sci. Rev.* **174**, 113-154 (2013).
45. Tian, F., Kasting, J. F. & Solomon, S. C. Thermal escape of carbon from the early Martian atmosphere. *Geophysical Research Letters* **36** (2009).
46. Terada, N. *et al.* Atmosphere and water loss from early Mars under extreme solar wind and extreme ultraviolet conditions. *Astrobiology* **9**, 55-70 (2009).
47. Ribas, I., Guinan, E. F., Gudel, M. & Audard, M. Evolution of the solar activity over time and effects on planetary atmospheres. I. High-energy irradiances (1-1700 angstrom). *Astrophysical Journal* **622**, 680-694 (2005).
48. Phillips, R. J. *et al.* Ancient geodynamics and global-scale hydrology on Mars. *Science* **291**, 2587-2591 (2001).
49. Wetzel, D. T., Rutherford, M. J., Jacobsen, S. D., Hauri, E. H., and Saal, A. E. Degassing of reduced carbon from planetary basalts. *Proceedings of the National Academy of Sciences of the United States of America* **110**, 8010-8013 (2013).
50. Zahnle, K., Haberle, R. M., Catling, D. C., and Kasting, J. F.. Photochemical instability of the ancient Martian atmosphere. *Journal of Geophysical Research-Planets* **113** (2008).

Requests for correspondence and additional materials should be addressed to Ramses Ramirez:

ramsesny@gmail.com

Acknowledgements

This paper benefited from reviews by Brian Toon, Robin Wordsworth, and an anonymous reviewer. We are grateful to Lee Kump for the tip on iron carbonyl. We also thank Vincent Eymet for providing KSPECTRUM. Support for this work came from the NASA Exobiology Program and the NASA Astrobiology Institute.

Individual contributions: RR and RK generated H₂O and CO₂ line-by-line cross-sections. RR generated CH₄ line-by-line cross sections with guidance from RF. RR performed most of the background research and climate model updates. RR and RK debugged the climate model. RR performed the computations and wrote most of Supp. Info. TR worked with RR in providing flux comparisons with SMART, and MZ performed numerical calculations of hydrodynamic escape rates. JK provided overall guidance and wrote much of the main text. All authors contributed to proof-reading and making comments on the paper.

SUPPLEMENTARY INFORMATION

1. CLIMATE MODEL DESCRIPTION

We used a 1-D radiative-convective climate model^{51,52,53} to study CO₂-H₂ greenhouse warming on early Mars. The current version of the model divides the atmosphere into 100 unevenly spaced layers in log pressure extending from the ground to a pressure of 3×10^{-5} bar. Radiative equilibrium is assumed for each layer in the stratosphere. At lower altitudes, if the radiative lapse rate within a layer exceeds the moist adiabatic lapse rate, then a convective adjustment is performed. The model relaxes to a moist H₂O adiabat at higher temperatures or to a moist CO₂ adiabat when it is cold enough for CO₂ to condense⁵⁴. This defines a convective troposphere near the surface. Within this troposphere, water vapor is assumed to be fully saturated for 9 out of our 10 simulations, thereby maximizing the greenhouse effect. (See main text, Fig. 2.) For the 95% CO₂/5% H₂ case, a sensitivity run with 50 percent relative humidity was performed to determine how much difference this would make. H₂O and CO₂ clouds are neglected in the model, but the effect of the former is accounted for by increasing the surface albedo, as done in previous climate simulations by our group^{53,54}. It has been argued that this methodology tends to overestimate the greenhouse effect of dense early atmospheres⁵⁵. By contrast, our neglect of CO₂ clouds may cause us to underestimate the greenhouse effect^{56,57}. Realistically determining the effect of clouds would probably require a 3-D climate model, and even then the cloud problem remains difficult.

Incident solar radiation and outgoing thermal infrared radiation are both treated using a two-stream approximation⁵⁸. Delta function scaling and the quadrature method are used at solar wavelengths. At those wavelengths, the model uses correlated-k coefficients to parameterize absorption by CO₂, H₂O and CH₄ across 38 spectral intervals ranging from 0.2 to 4.5 microns. In

the solar, we currently use 8-term CO₂ k-coefficients derived from HITRAN 2008, whereas our 8-term H₂O coefficients utilize HITRAN 2008 at low pressures and HITEMP 2010 for pressures greater than or equal to 0.1 bar⁵⁹. The near-IR CH₄ coefficients for wavelengths less than 1 μm are those derived from Karkoschka⁶⁰, whereas those longward of 1 μm were derived from self-broadened k-distributions⁶¹. These latter coefficients were interpolated between 188 K and 295 K. These CO₂, and H₂O coefficients, and the thermal-IR ones described below, have replaced those used in our other recent studies of early Mars^{57,62}, and they produce excellent agreement in both the upwelling and downwelling thermal-IR fluxes when compared against both the well-tested SMART line-by-line model⁶³ and Fig. 2c of Wordsworth et al.⁶⁴ for the same dense CO₂ atmosphere used by the latter authors (see Fig. S1-S5).

In the thermal infrared, 8-term k-coefficients are used for CO₂ and H₂O⁵⁹ and new 4-term coefficients have been derived for CH₄ in 55 spectral intervals extending from 0 – 15,000 cm⁻¹. The coefficients for CO₂ and H₂O were calculated using line width truncations of 500 cm⁻¹ and 25 cm⁻¹, respectively, and were computed over 8 temperatures (100, 150, 200, 250, 300, 350, 400, 600 K) and 8 pressures (10⁻⁵ – 100 bar). A short truncation width was used for H₂O because we overlaid this with a continuum, as described below. The CH₄ coefficients (truncated at 35 cm⁻¹) were computed at the same 8 pressures and the following 5 temperatures (100,200,300,400,600) K. Overlap between gases was computed by convolving the k-coefficients within each broadband spectral interval.

We use the 4.3 micron CO₂ chi factors of Perrin and Hartmann⁶⁵ as a proxy for CO₂ far wing absorption in the 15 micron region. For water, the BPS continuum of Paynter and Ramaswamy⁶⁶ is overlain over its entire range of validity (0 – 19,000cm⁻¹).

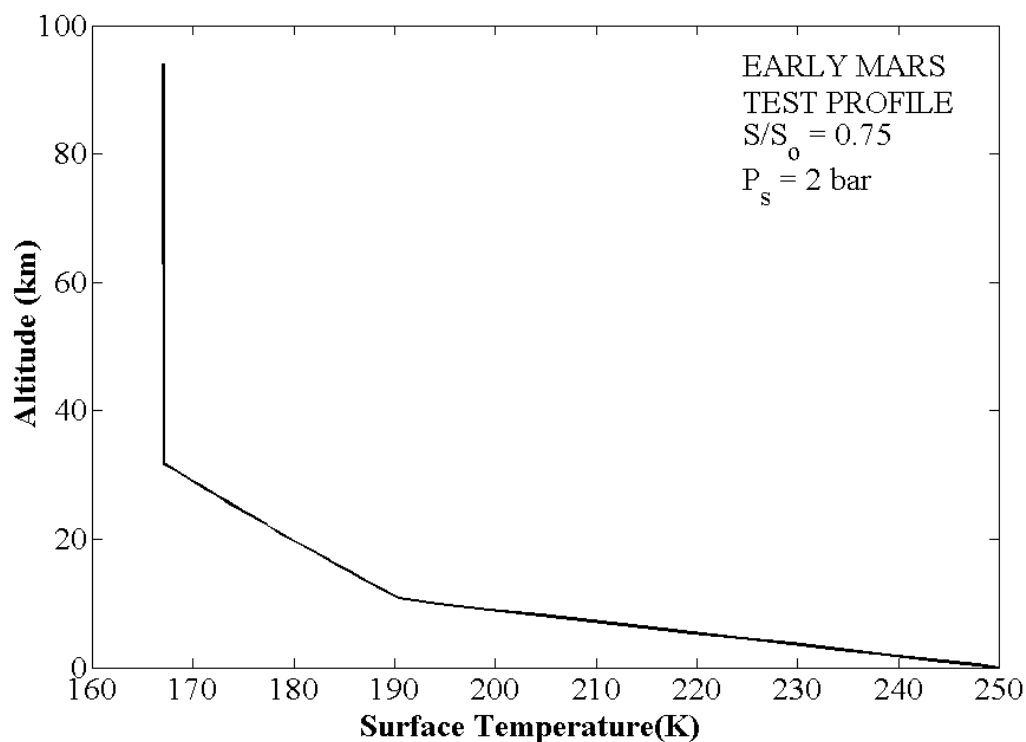


Figure S1: Temperature-pressure profile for a 2-bar 95% CO₂ 5 % N₂ dry atmosphere with early Mars insolation ($S/S_0 = 0.75$) used for flux comparisons in Fig. S2- S5. The surface temperature is 250 K and stratospheric temperature is fixed at 167K. This test profile is not an output of the nominal runs in the main text.

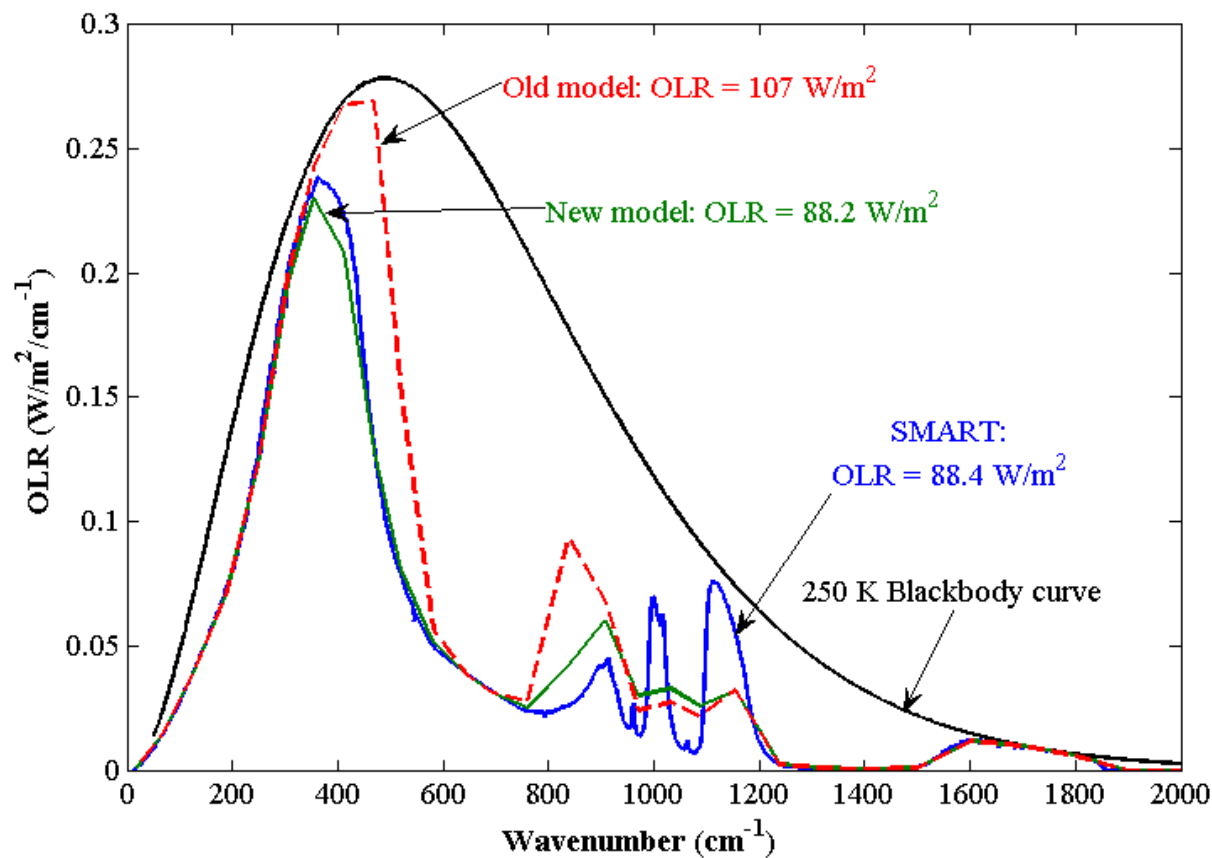


Figure S2: Emission spectra for the atmosphere in Fig. S1, comparing (a) the old model CO_2 coefficients against those of both (b) the new model (this paper), and (c) the line-by-line model SMART⁶³. All three models use the GBB CO_2 CIA parameterization.^{73,74,75} Our computed outgoing longwave radiative (OLR) flux (88.2 W/m^2) is in excellent agreement with Wordsworth et al.⁶⁴ Fig 2c and comes to within $\sim 0.2\%$ of SMART. Slight differences between our new model and SMART are attributable to spectral resolution differences and different assumptions about line profiles. Our model uses Voigt line profiles, whereas SMART utilizes van Vleck-Weisskopf and Rautian line profiles. Our old model underestimates CO_2 absorption by $\sim 20 \text{ W/m}^2$ because of relatively short line truncation ($\sim 25 \text{ cm}^{-1}$), which neglects much of the far wing contribution at higher pressures⁷². Note that previous simulations by our group using the old model^{52,53,62} had implemented the Kasting et al.⁵¹ CO_2 CIA parameterization, which overestimated continuum absorption. Here, we decided to use the GBB CO_2 CIA parameterization for ease of comparison with all three cases.

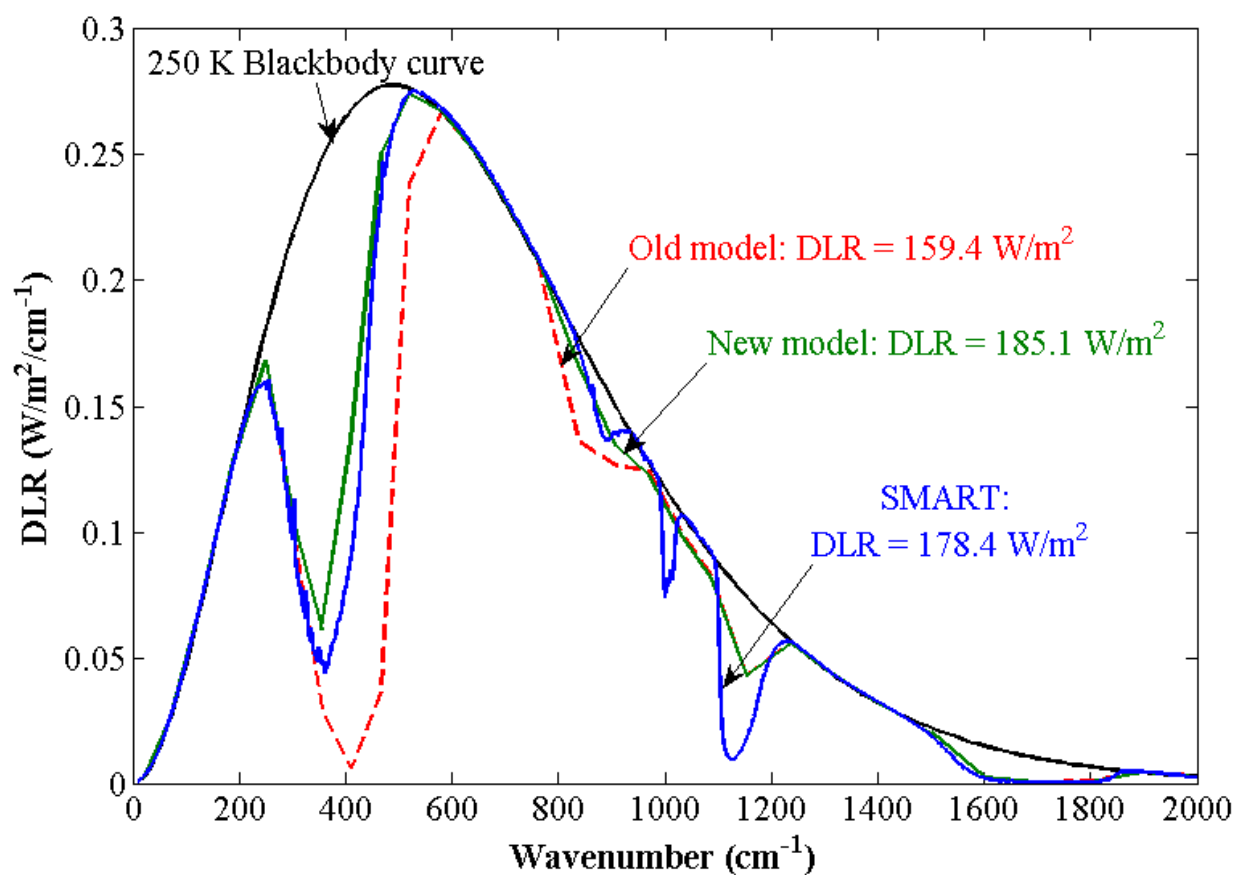


Figure S3: Surface downwelling longwave radiative (DLR) spectral flux comparisons for the atmosphere in Fig. S1. The longer CO₂ line shapes used by both our new model and by SMART explain the ~14% and 11% higher surface downwelling fluxes, respectively, as compared to our old model. Our slightly larger (~3.6%) surface flux as compared to SMART is likely due to the line profile differences discussed in the caption to Fig. S2.

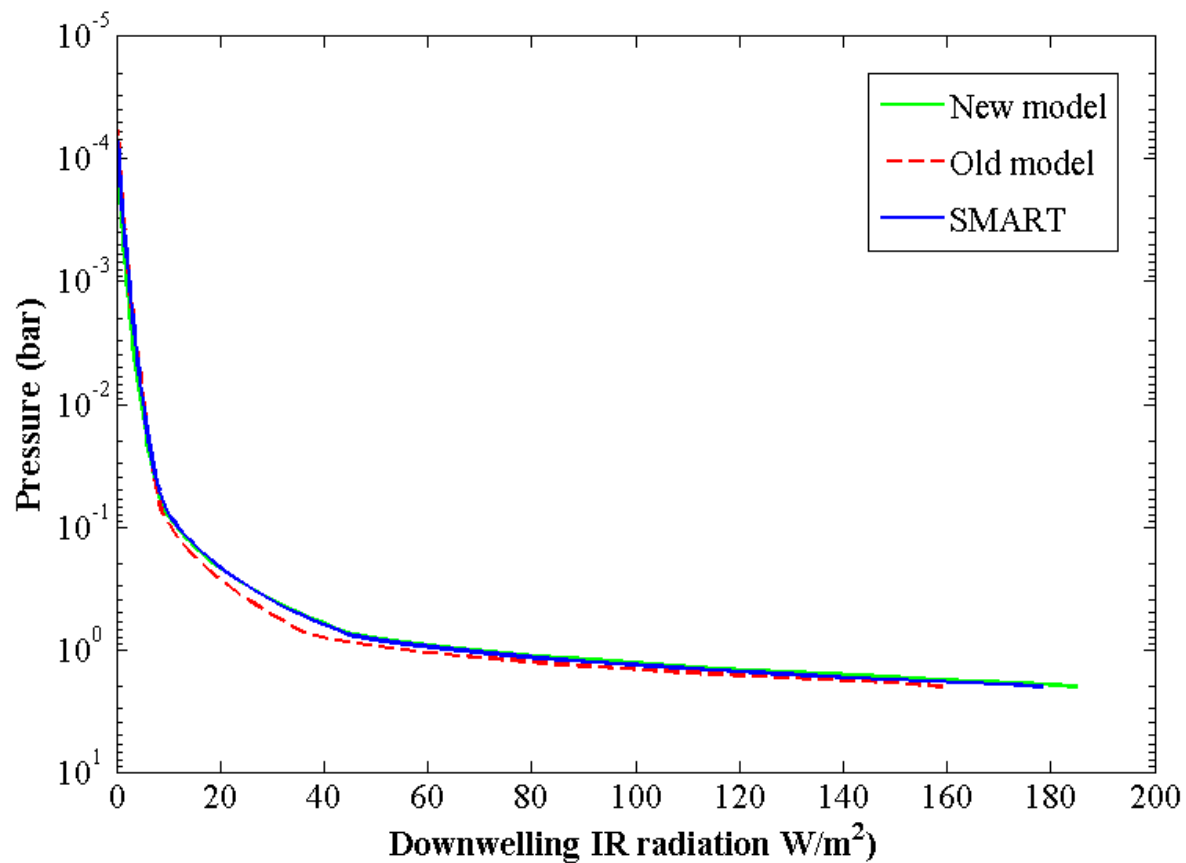


Figure S4: Downwelling longwave radiative (DLR) broadband flux comparisons for the atmosphere in Fig. S1. Fluxes calculated by SMART and by our new model agree well at most heights, although our model has a slightly stronger ($\sim 3.6\%$) greenhouse effect at the surface.

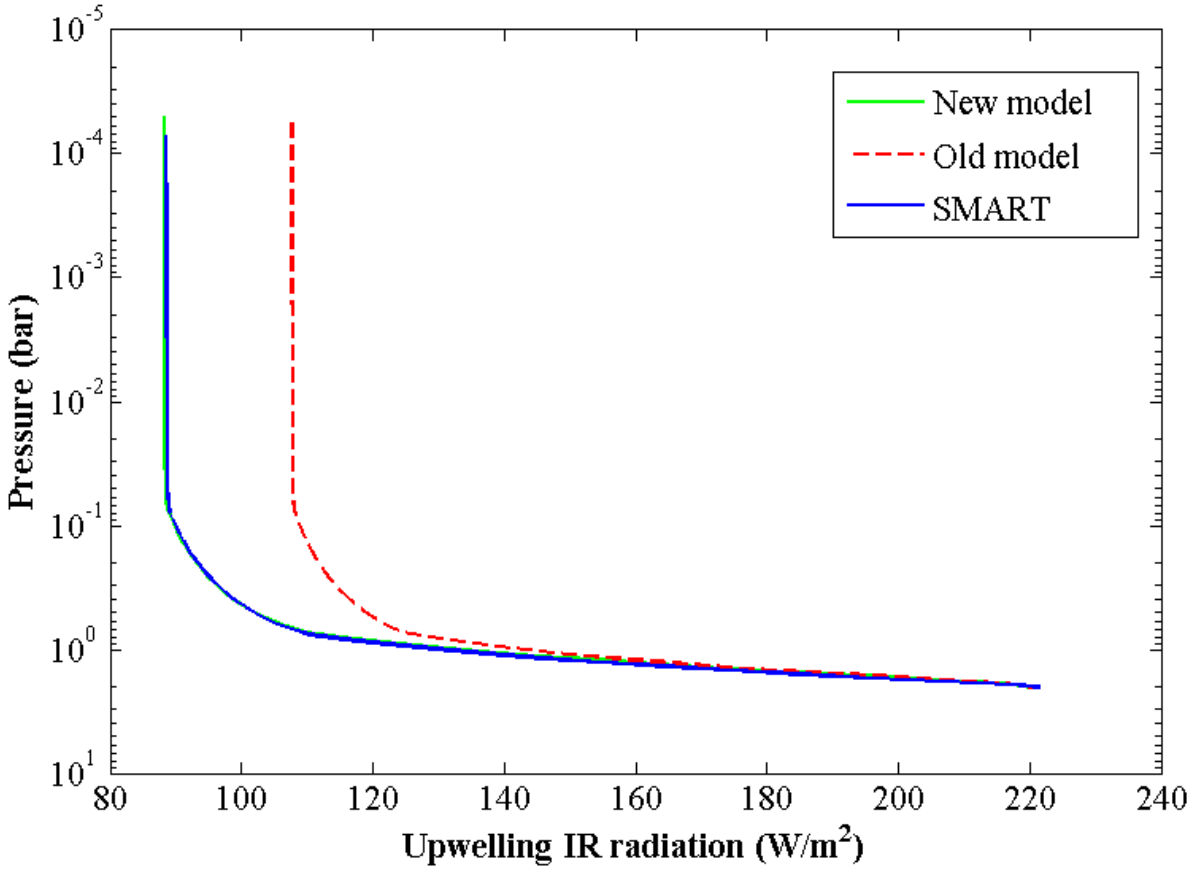


Figure S5: Upwelling longwave radiative broadband flux comparisons for the atmosphere in Fig. S1. Our new model is in excellent agreement with SMART at all heights, whereas the flux calculated by our old model is higher by as much as 19.4 W/m^2 in the stratosphere.

The following additional updates were made to the climate model:

1) We included collision-induced absorption (CIA) caused by the interaction of H_2 with CO_2 .

CO_2 is an anisotropic molecule that picks up a strong dipole moment when its bending mode is activated, necessitating extra quantum mechanical treatments that are at this stage considered experimental (L. Frommhold, personal communication). Therefore, we modeled $\text{CO}_2\text{-H}_2$ CIA using measured absorption coefficients for $\text{N}_2\text{-H}_2$ CIA⁶⁷. We believe that this approach is conservative, as Burch et al.⁶⁸ determined that self-broadening of permitted CO_2 transitions was ~30% more effective than foreign-broadening by N_2 . The relatively small moment of inertia for

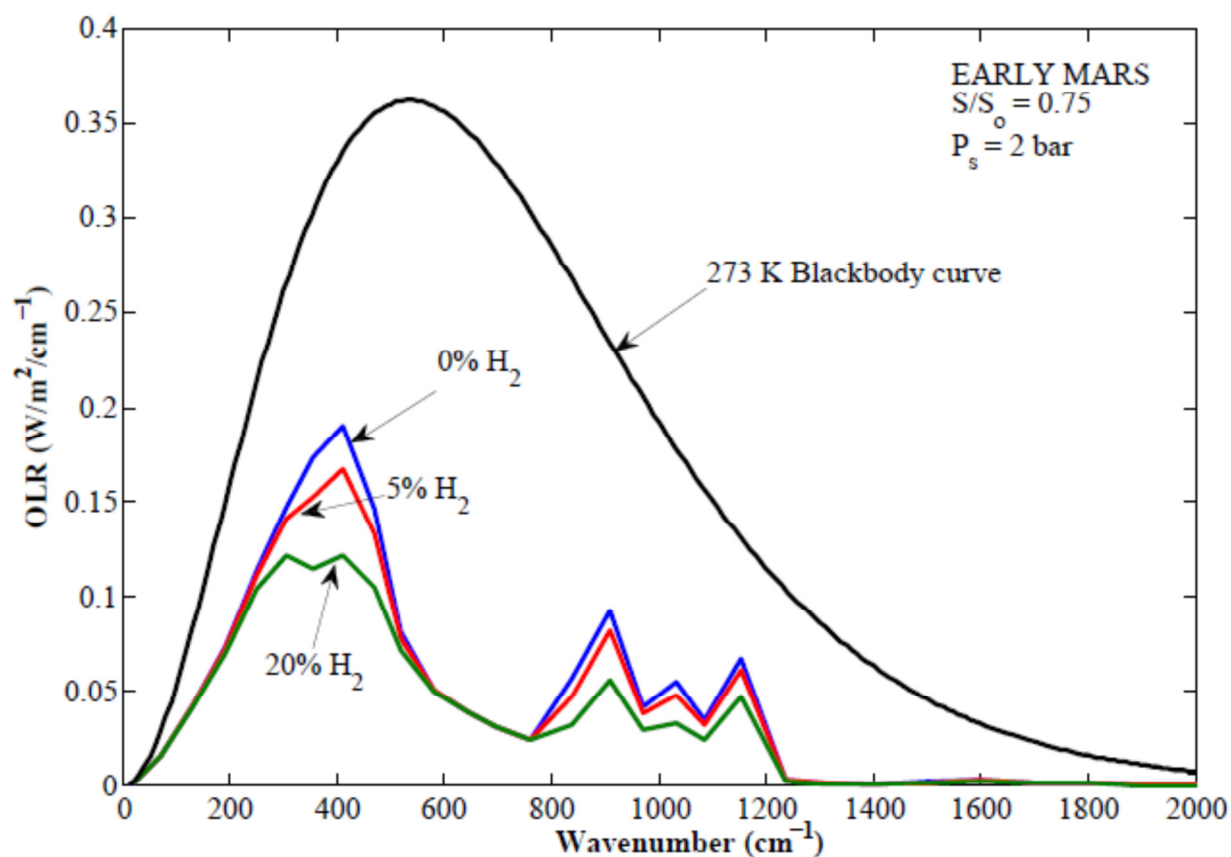


Figure S6: Emission spectrum for a 2-bar early Mars ($S/S_o = 0.75$) atmosphere containing 95% CO₂ and 5% N₂ (blue), 95% CO₂ and 5% H₂ (red), or 80% CO₂ and 20% H₂ (green). The surface temperature is 273K, and the stratospheric temperature is fixed at 167 K. Adding 5% and 20% H₂ reduces the outgoing infrared flux by ~ 6 W/m² and 22 W/m², respectively. Vertical infrared flux profiles for these cases are shown in Fig. S7.

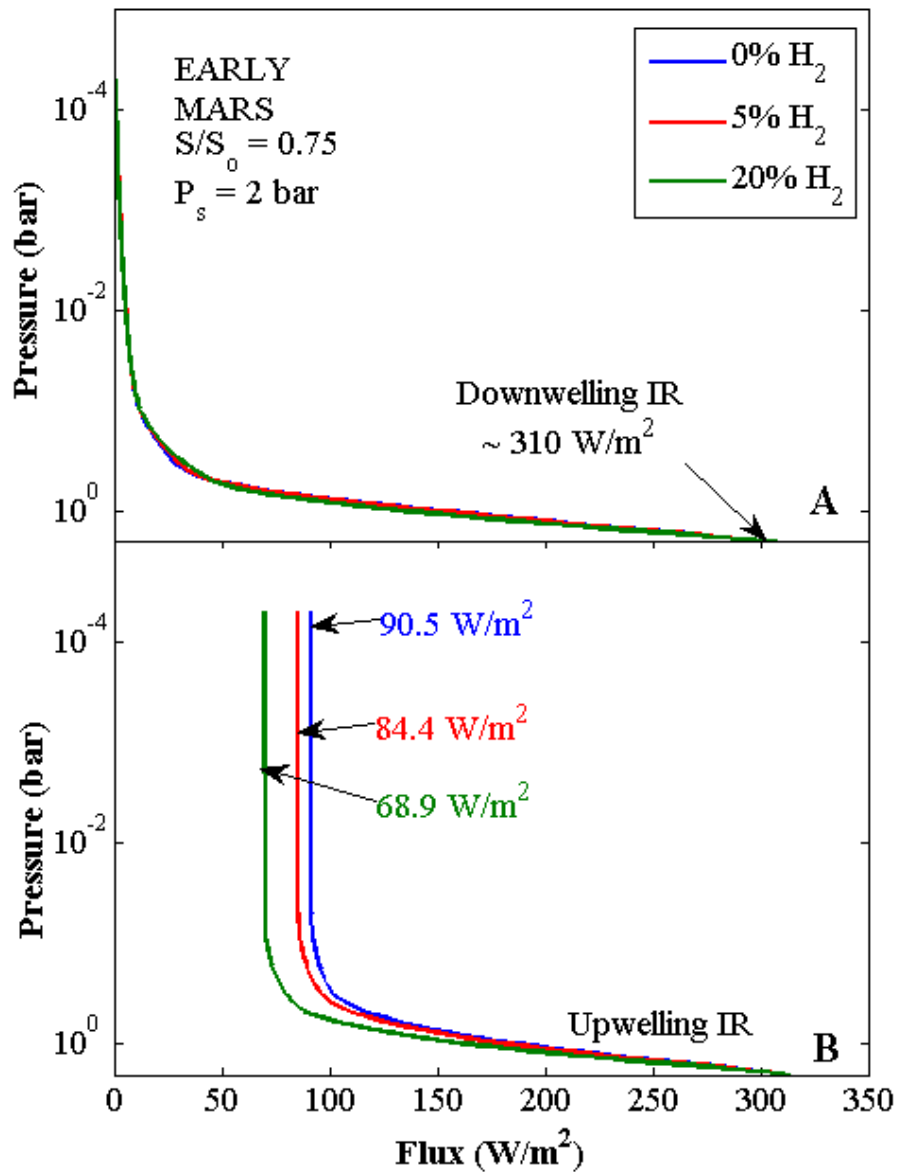


Figure S7: Infrared (IR) flux profiles for the 2-bar, 273 K surface temperature atmosphere shown in Figure S6. Although all scenarios yielded a similar downwelling IR flux, the 5% and 20% H_2 cases resulted in ~ 6 and 22 W/m^2 reductions in upwelling IR, respectively, greatly enhancing the greenhouse effect. Coupled with a strong CO_2 greenhouse effect, these radiative forcings from H_2 increase atmospheric temperatures above freezing.

H₂, coupled with its widely-spaced rotational levels, results in absorption over a large swath of the thermal infrared, including the 200-600 cm⁻¹ and the 8-12 micron regions⁶⁹ (See Figs. S6 and S7).

Indeed, collision-induced absorption by H₂ broadened by other molecules such as Ar, N₂, or even itself, all produce absorption over the same spectral range⁷⁰. Subsequently, the same would be true for CO₂-H₂. Although CO₂ is more effective at Rayleigh scattering than is N₂, our CO₂-H₂ cases still produce more surface warming than does our N₂-H₂ case (Fig. 2, main text). Thus, the increase in Rayleigh scattering as CO₂ increases is outstripped by increased absorption within the 15 micron band. This suggests that CO₂ would have to broaden H₂ considerably less effectively than N₂ does for our mechanism to fail, contrary to the available evidence⁶⁸. Consequently, we use the N₂-H₂ CIA data of Borysow and Frommhold⁶⁷ as a lower bound for the calculation of CO₂-H₂ opacity (τ_l). This lower bound parameterization is then:

$$\tau_l = H_i \frac{n}{n_o} W_{H_2} f_{CO_2} \quad (S1)$$

Here, H_i is a constant (see below) with units of amagat⁻² cm⁻¹, W_{H_2} is the H₂ path length in atmosphere-centimeters, n is number density, n_o is Loschmidt's constant (2.687×10¹⁹ molecules/atm-cm³), and f_{H_2} is the H₂ mixing ratio. The quantity f_{CO_2} represents the foreign broadening by CO₂. This lower bound estimate resulted in mean surface temperatures above 273 K at ~ 2.5 bar for 10% H₂ and ~1.5 bar for 20% H₂.

The N₂-H₂ collision-induced absorption coefficients, H_i , used in Eq. S1 are tabulated below (Table I). N₂-H₂ CIA coefficients, like other absorption coefficients in our model, are interpolated log-linearly (linear in T , logarithmic in the absorption coefficient) between the values shown in Table I.

2) We also incorporated self-broadening by H₂-H₂ pairs⁷¹, using the following equation for the opacity, τ_p :

$$\tau_p = H_i \frac{n}{n_o} W_{H_2} f_{H_2} \quad (S2)$$

Inspection of Equations S1 and S2 reveals that self-broadening by H₂ is less important than foreign-broadening when H₂ is the secondary greenhouse gas. This is because the pathlength (W_{H_2}) is a linear function of the mixing ratio, and τ_p is a quadratic function of f_{H_2} . In contrast, τ_l is approximately linear in f_{H_2} at low mixing ratios. Furthermore, a comparison of the tabulated data for self- and foreign-broadening of H₂ (Tables I and II, respectively) shows that H₂ foreign broadening is generally more effective at any given temperature and frequency. We conducted a sensitivity study to quantify the effect of removing the H₂ self-broadening component. Our results showed that the maximum surface temperatures obtained in Figure 2 (main text) decreased by no more than 2-3 degrees when this was done.

3) Both Halevy et al.⁷² and Wordsworth et al.⁶⁴ have pointed out that our old climate model, which was derived from that of Kasting et al.⁵¹, may have significantly overestimated absorption of thermal-IR radiation by CIA bands of CO₂. Consequently, we replaced our old CO₂ CIA parameterization with the one described in Wordsworth et al.⁶⁴. CO₂ CIA becomes significant at higher pressures and consists of two separate effects: 1) close collisions between CO₂ molecules that induce temporary dipoles, and 2) colliding molecules that form CO₂-CO₂ dimers. These two phenomena result in the creation of new absorption bands^{73,74,75}. Our revised parameterization (hereafter, GBB after ref. 64) computes the optical depth (τ_{CO_2}) from the following formula:

$$\tau_{co_2} = C_i \frac{n}{n_o} W_{co_2} \quad (S3)$$

Here C_i is a constant (see below) with units of $\text{amagat}^{-2} \text{ cm}^{-1}$, and W_{CO_2} is the CO_2 pathlength in atmosphere-centimeters.

The new CO_2 - CO_2 collision-induced absorption coefficients, C_i , used in Eq. S3 are tabulated below (Table III). Within the $0\text{--}495 \text{ cm}^{-1}$ spectral region we replaced the calculated values at 150 K with those at 200 K. We did this because the model of Gruszka and Borysow^{73,74} may be unreliable below $\sim 200 \text{ K}$. However, because the pressures associated with such temperatures are very small on Mars, collisions should be very infrequent. Thus, CIA is unimportant at these lower temperatures and our results are insensitive to the absorption coefficient values at $T = 150 \text{ K}$.

4) We also incorporated near-IR CO_2 CIA from the 1.2, 1.73, and 2.3 micron regions using tabulated values from previous Venusian studies⁷⁶⁻⁷⁹. The temperature dependence of near-IR CO_2 CIA is difficult to measure experimentally and the values are poorly known. However, as the resultant optical depths were of order 10^{-4} to 10^{-3} , these bands had only a small effect on our simulations.

5) The Shomate Equation (<http://www.vscht.cz/fch/cz/pomucky/fchab/Shomate.html>) was used to calculate new heat capacity relationships for CO_2 , H_2 , and H_2O . Notably, at low temperatures, c_p for CO_2 decreased by $\sim 30\%$ relative to values in our previous model. This increased the dry adiabatic lapse rate, g/c_p , by an equivalent amount but had surprisingly little effect on computed surface temperatures, apparently because the steeper lapse rate in the upper troposphere was largely compensated by a decrease in tropopause height. (As mentioned earlier, our model assumes a moist adiabatic lapse rate, but this relaxes to a dry adiabat in regions where CO_2 is not condensing and where H_2O is scarce).

- 6) Our climate model now includes Rayleigh scattering by H_2 ⁸⁰. This addition had a negligible effect on our results.
- 7) The Rayleigh scattering coefficient of water vapor was taken from measured values⁸¹⁻⁸³. Our previous climate model had used the same value as for air. Again, this had only a small effect on the results, because H_2O is always a minor constituent in these calculations. But the effect of this change on a warm, moist atmosphere would be significant, as the coefficient for H_2O is ~30% lower than that for air.
- 8) Our new model now incorporates the decrease of gravity with altitude, which tends to slightly decrease thermal infrared emission, because as the gravity decreases, the optical depth at a given pressure level increases. This effect is more pronounced for smaller planets such as Mars⁵⁹.
- 9) Our model can now perform calculations involving multiple solar zenith angles, increasing the accuracy of shortwave absorption. We performed a sensitivity study using 6 gauss points, which slightly decreases the H_2 and pCO_2 thresholds required to reach the freezing point (Fig. S8).

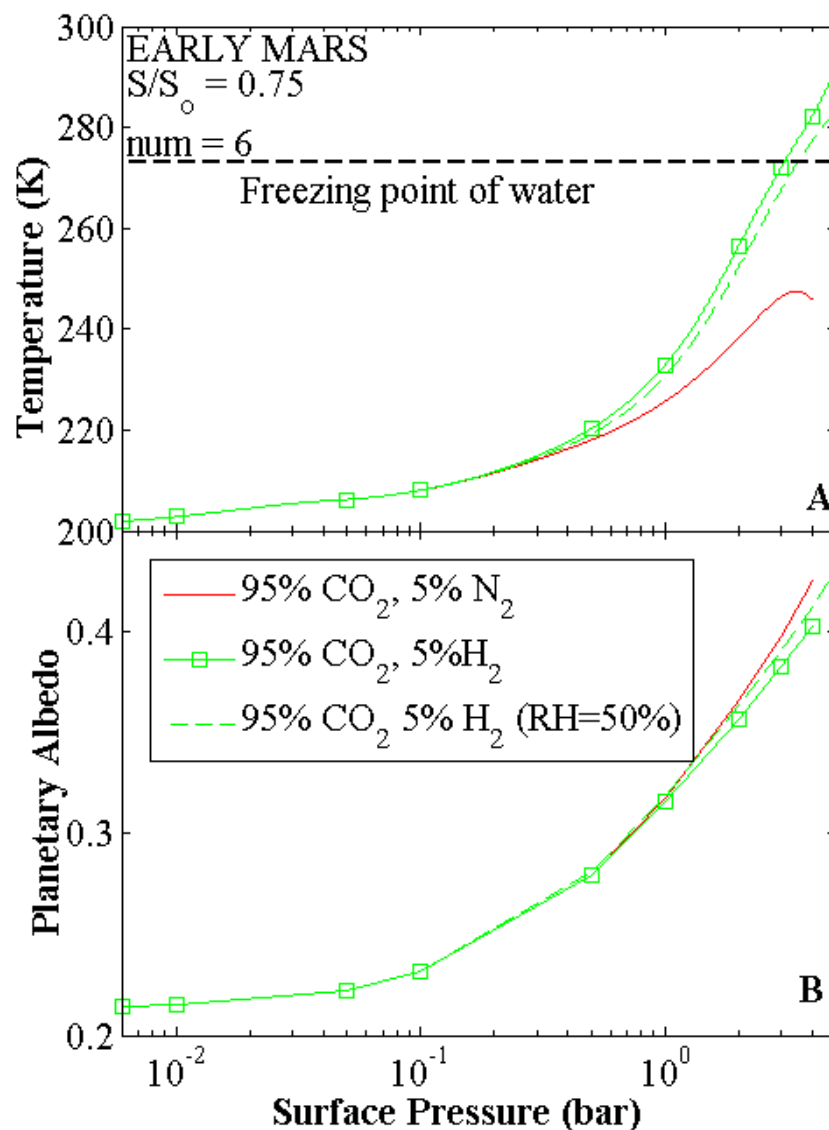


Figure S8: Surface temperature and planetary albedo as a function of surface pressure for two 95% CO_2 , fully-saturated early Mars ($S/S_0 = 0.75$) atmospheres containing (a) 5% N_2 , (b) 5% H_2 , and (c) 5% H_2 with a relative humidity of 50%. The assumed surface albedo is the same as that used in Fig. 2 of the main text. A 6-point gaussian integration scheme was used over the sun-lit hemisphere (num = 6). The cosine-weighted average solar flux factor was ~ 0.503 , which compares to the true value of 0.50. The mean temperature for the baseline 5% N_2 case rose from 230 K (Fig. 2 in main text) to 246 K here. With six gauss points, even the 50% relative humidity scenario reaches the freezing point with 5% H_2 and just under ~ 3 bars total surface pressure.

2. OUTGASSING OF H₂ AND THE ATMOSPHERIC REDOX BUDGET

As discussed in the main text, H₂ and other reduced gases should have been outgassed from the reduced martian mantle. The H₂:H₂O ratio in these gases would have been determined by reaction (1) in the main text: $2 \text{H}_2\text{O} \xrightleftharpoons{K_1} 2 \text{H}_2 + \text{O}_2$, for which the equilibrium constant K_1 is given by

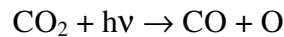
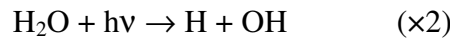
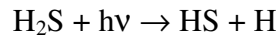
$$K_1 = \frac{p_{\text{H}_2}^2 \cdot f_{\text{O}_2}}{p_{\text{H}_2\text{O}}^2} = e^{-\Delta G_1^0 / (RT)} \quad (\text{S4})$$

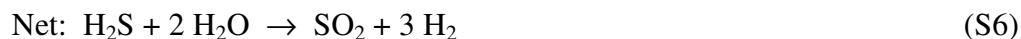
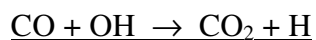
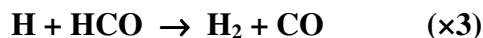
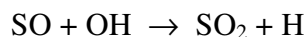
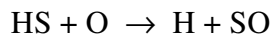
Here, ΔG_1^0 is the change in Gibbs free energy for the reaction at standard state. The free energies of formation of H₂ and O₂ are defined as zero at all temperatures. Using data from the NIST-JANAF thermochemical tables⁸⁴, the free energy of formation of H₂O at 1200°C is $\Delta G_f^0(\text{H}_2\text{O}) = -165.58 \text{ kJ/mol}$, so the free energy change for the reaction is just

$$\Delta G_1^0 = -2 \cdot \Delta G_f^0(\text{H}_2\text{O}) = 331.16 \text{ kJ/mol} \quad (\text{S5})$$

Using Eq. S4 above, the equilibrium constant at 1200°C is $K_1 \cong 1.80 \times 10^{-12} \text{ atm}$. This value of the equilibrium constant is used in the main text.

So far, we have only accounted for H₂ itself. But, other reduced gases also enter into the atmospheric redox budget, because they can be oxidized by the byproducts of H₂O and CO₂ photolysis to produce H₂. By adopting a methodology in which certain gases (H₂O, CO₂, N₂, and SO₂) are assigned “neutral” oxidation states, one can evaluate the contribution of other gases to the atmospheric redox budget^{85,86}. For example, H₂S can be converted to SO₂ and H₂ by the reaction sequence (see reaction rates in ref. 87)





This net reaction is the same one quoted in the main text. The particular reaction sequence shown here is by no means the only one that would have operated in the primitive atmosphere, but it is a particularly effective one because the two boldface reactions provide a catalytic cycle for producing H_2 (ref. 88). H_2S can also react directly with OH to produce $\text{H}_2\text{O} + \text{HS}$, and H can react with HS to produce $\text{H}_2 + \text{S}$. Regardless of how the actual reaction path proceeds, each mole of H_2S outgassed is equivalent to 3 moles of outgassed H_2 , if the sulfur is removed as SO_2 . If the H_2S is oxidized to sulfate, then an additional mole of H_2 is produced. Similarly, for CH_4 and CO , we can write



Thus, one mole of CH_4 yields 4 moles of H_2 , and one mole of CO yields one mole of H_2 .

All three of these additional reduced gases would have helped to build up the inventory of atmospheric H_2 . In the main text, we estimated the rate of H_2 outgassing on early Mars by making an analogy to modern Earth, and we assumed that outgassing of H_2S scaled proportionately with H_2 . For the carbon-bearing gases, we can make a similar analogy to modern Earth. On Earth, the main carbon-bearing volcanic gas is CO_2 , for which the estimated global release rate is $(7.5 \pm 2) \times 10^{12} \text{ mol/yr}$ ⁸⁹, or $\sim 2.8 \times 10^{10} \text{ cm}^{-2} \text{ s}^{-1}$. (We will use areal outgassing rates

here, so as not to have to account for the different surface areas of Earth and Mars.) On early Mars, because of the planet's reduced mantle, carbon would have been outgassed as a combination of CO and CH₄⁹⁰. Wetzel et al. estimate that initial crustal formation would have released 1 bar of CO and 1.3 bar of CH₄. By converting from partial pressure to volume units (thereby accounting for the mass of O and H), we calculate that 30% of the outgassed carbon would have been released as CO, and 70% would have been released as CH₄. If we assume that early Mars outgassed carbon at the same rate per unit area as modern Earth—the same assumption made in the main text for total hydrogen--the equivalent H₂ outgassing rate can be estimated by multiplying the CO₂ outgassing rate given above by 0.3 for CO and by 0.7×4 for CH₄, where the factor of 4 comes from the stoichiometry of reaction S7. The net equivalent outgassing of H₂ is then $8.7 \times 10^{10} \text{ cm}^{-2} \text{ s}^{-1}$. By comparison, the estimates given for combined (H₂ + H₂S) outgassing in the main text were $1 \times 10^{10} \text{ cm}^{-2} \text{ s}^{-1}$ for modern Earth, $2 \times 10^{11} \text{ cm}^{-2} \text{ s}^{-1}$ for early Mars at a mantle $f\text{O}_2$ of IW+1, and $4 \times 10^{11} \text{ cm}^{-2} \text{ s}^{-1}$ for early Mars at IW–1. So, outgassing of CH₄ and CO would have made an appreciable, but not dominant, contribution to the atmospheric redox budget of early Mars.

3. EFFECT OF CH₄ ON CLIMATE IN A DOMINANTLY CO₂-H₂ EARLY MARS ATMOSPHERE

As discussed above, if Mars' early mantle was highly reduced, some C would have been outgassed in the form of CH₄. Thus, CH₄ would be expected to have contributed to the greenhouse effect. Here, we assess the climate effect of adding 1% CH₄ and various combinations of CO₂ and H₂ to representative fully-saturated 3-bar atmospheres with a surface temperature of 230 K. The instantaneous radiative forcing, defined here as the reduction in

outgoing infrared radiation at the top of the atmosphere, caused by such an addition is shown in Table IV. Any remaining gas in these calculations is assumed to be N₂. In all cases, the additional radiative forcing from CH₄ is no more than 1 W/m². By comparison, H₂ absorption produced 6 - 22 W/m² forcing for H₂ concentrations of 5-20% (Fig. S6).

Selected temperature-altitude profiles for the 95% CO₂, 5% H₂ case are given in Fig. S9. H₂O and CO₂ cloud-forming regions are shown for the 3-bar case. Clouds are not included explicitly in the radiative transfer model, but their formation does affect the tropospheric lapse rate. As noted above, the greenhouse contribution from CH₄ is expected to be small in a dense CO₂ early Mars atmosphere. However, CH₄ absorbs strongly in the near-IR and could have contributed significantly to heating of the mid and upper atmosphere, thereby inhibiting CO₂ cloud formation (Fig. S10). As previous studies^{56,57,91} have suggested that backscattering from CO₂ ice clouds would warm the surface under high fractional cloud cover (≥ 0.5), this could conceivably result in surface cooling as compared to the zero-CH₄ case, but perhaps not by that much, as a recent study⁹² suggests that the two-stream method may have overestimated the warming coming from the backscatter of CO₂ ice crystals. To determine how important this process might be, this effect should be investigated with a more elaborate 3-D climate model that includes clouds, such as the model described in refs. 13 and 14 in the main text.

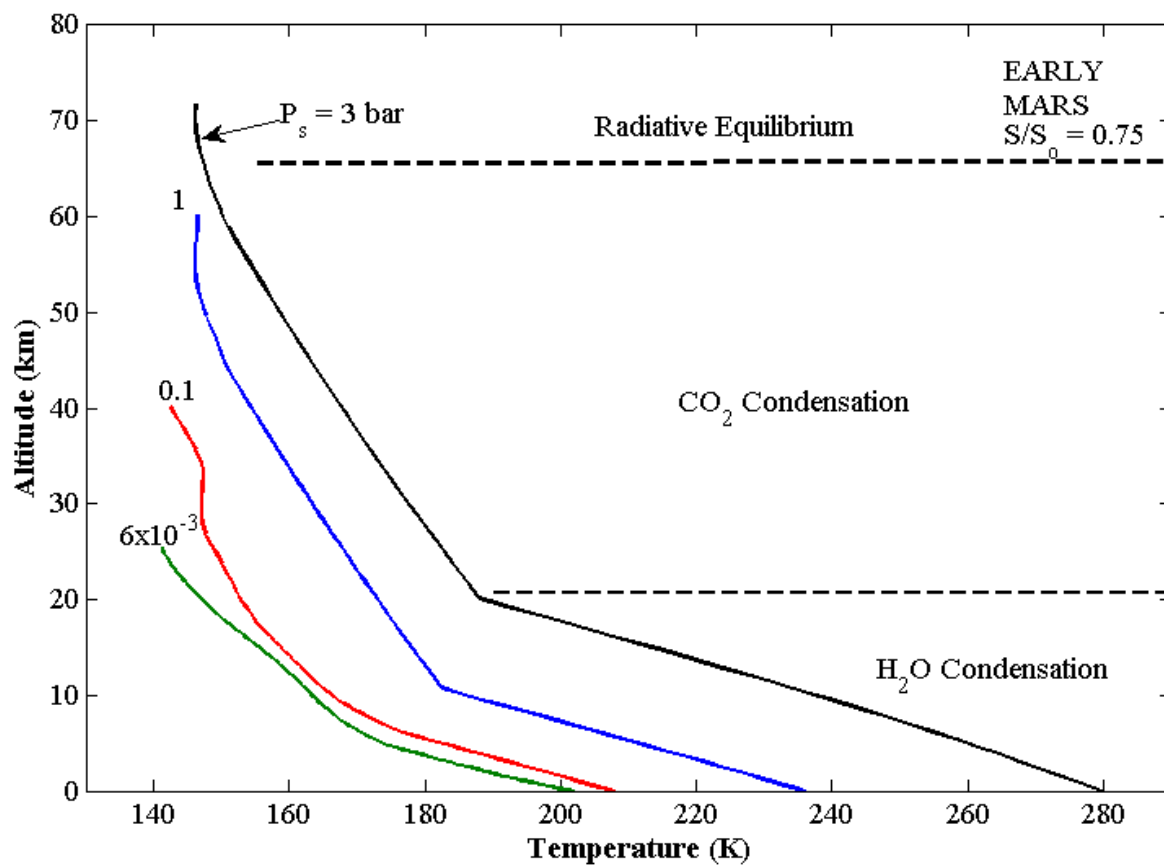


Figure S9: Selected vertical temperature profiles for the fully-saturated 95% CO₂ 5% H₂ case shown in Fig. 2 of the main text. As the total atmospheric pressure increases from 6×10^{-3} to 3 bar, the magnitude of the greenhouse effect from the combined effects of the CO₂ greenhouse and H₂ collision-induced absorption, is ~ 70 degrees.

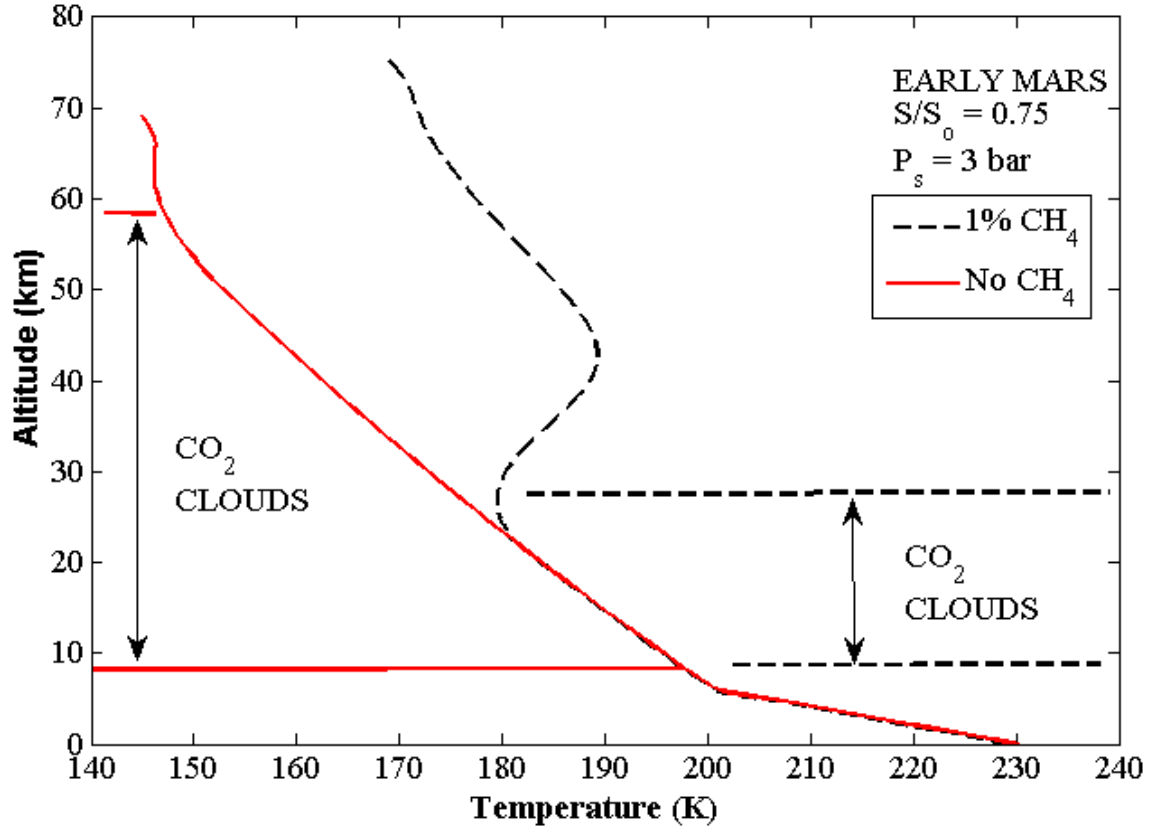


Figure S10: Temperature-altitude profiles for fully-saturated 3-bar CO₂ early Mars ($S/S_0 = 0.75$) atmospheres with (a) 1% CH₄ and (b) no CH₄. The surface albedo is the same as in Fig. 2 in the main text. The calculated surface temperature is ~230 K in both cases. Addition of 1% CH₄ has little direct effect on surface temperature, but it decreases the size of the CO₂ cloud deck from ~50 km to ~20 km. This effect may prove important in 3D GCMs that include clouds and in assessing the intensity of CO₂ condensation at the poles and at higher elevations. Sensitivity studies that included both self-broadened and foreign-broadened CH₄ CIA (assuming CO₂-CH₄ broadens as well as N₂-CH₄) had a small effect, increasing surface temperatures to just over 231 K. The CH₄ self-broadening component is small because CH₄ composes only 1% of the atmosphere. N₂-CH₄ CIA band absorbs most strongly in the far-IR, which is masked by the pure rotation band of water.

4. TABLES OF CIA DATA

Table IA: N₂-H₂ Collision-induced absorption coefficients in the 0 - 1000 cm⁻¹ spectral range.

	T = 150K	T = 200K	T = 300K
Wavenumber interval (cm⁻¹)	CIA (amagat⁻²cm⁻¹)	CIA (amagat⁻²cm⁻¹)	CIA (amagat⁻²cm⁻¹)
0 - 40	6.32x10 ⁻⁷	4.33x10 ⁻⁷	2.54x10 ⁻⁷
40 - 100	2.63x10 ⁻⁶	2.03x10 ⁻⁶	1.35x10 ⁻⁶
100 - 160	3.08x10 ⁻⁶	2.92x10 ⁻⁶	2.45x10 ⁻⁶
160 - 220	2.00x10 ⁻⁶	2.24x10 ⁻⁶	2.41x10 ⁻⁶
220 - 280	1.73x10 ⁻⁶	1.94x10 ⁻⁶	2.17x10 ⁻⁶
280 - 330	4.26x10 ⁻⁶	3.58x10 ⁻⁶	2.89x10 ⁻⁶
330 - 380	1.13x10 ⁻⁵	7.42x10 ⁻⁶	4.45x10 ⁻⁶
380 - 440	7.13x10 ⁻⁶	5.50x10 ⁻⁶	4.07x10 ⁻⁶
440 - 495	3.93x10 ⁻⁶	4.19x10 ⁻⁶	4.36x10 ⁻⁶
495 - 545	7.84x10 ⁻⁶	8.77x10 ⁻⁶	8.60x10 ⁻⁶
545 - 617	2.78x10 ⁻⁵	2.46x10 ⁻⁵	1.85x10 ⁻⁵
617 - 667	1.87x10 ⁻⁵	1.82x10 ⁻⁵	1.54x10 ⁻⁵
667 - 720	7.47x10 ⁻⁶	8.44x10 ⁻⁶	8.84x10 ⁻⁶
720 - 800	3.24x10 ⁻⁶	4.47x10 ⁻⁶	5.91x10 ⁻⁶
800 - 875	2.72x10 ⁻⁶	4.07x10 ⁻⁶	5.62x10 ⁻⁶
875 - 940	9.67x10 ⁻⁷	1.73x10 ⁻⁶	3.22x10 ⁻⁶
940 - 1000	4.60x10 ⁻⁷	1.10x10 ⁻⁶	3.03x10 ⁻⁶

Table IB: N₂-H₂ Collision-induced absorption coefficients in the 1000 - 2050 cm⁻¹ spectral range.

	T = 150K	T = 200K	T = 300K
Wavenumber interval (cm⁻¹)	CIA (amagat⁻²cm⁻¹)	CIA (amagat⁻²cm⁻¹)	CIA (amagat⁻²cm⁻¹)
1000 - 1065	5.07x10 ⁻⁷	1.53x10 ⁻⁶	4.45x10 ⁻⁶
1065 - 1108	3.05x10 ⁻⁷	1.02x10 ⁻⁶	3.33x10 ⁻⁶
1108 - 1200	1.19x10 ⁻⁷	3.99x10 ⁻⁷	1.55x10 ⁻⁶
1200 - 1275	4.43x10 ⁻⁸	1.43x10 ⁻⁷	7.03x10 ⁻⁷
1275 - 1350	2.03x10 ⁻⁸	6.40x10 ⁻⁸	3.56x10 ⁻⁷
1350 - 1450	9.02x10 ⁻⁹	2.59x10 ⁻⁸	1.74x10 ⁻⁷
1450 - 1550	6.50x10 ⁻⁹	1.38x10 ⁻⁸	9.44x10 ⁻⁸
1550 - 1650	1.63x10 ⁻⁸	1.81x10 ⁻⁸	4.35x10 ⁻⁸
1650 - 1750	1.45x10 ⁻⁸	1.53x10 ⁻⁸	2.53x10 ⁻⁸
1750 - 1850	5.69x10 ⁻⁹	7.19x10 ⁻⁹	1.26x10 ⁻⁸
1850 - 1950	2.15x10 ⁻⁸	3.18x10 ⁻⁹	6.29x10 ⁻⁹
1950 - 2050	1.40x10 ⁻⁹	2.3x10 ⁻⁹	4.49x10 ⁻⁹

Table IIA: H₂-H₂ Collision-induced absorption values in the 0- 1000 cm⁻¹ spectral range.

	T = 150K	T = 200K	T = 300K
Wavenumber interval (cm⁻¹)	CIA (amagat⁻²cm⁻¹)	CIA (amagat⁻²cm⁻¹)	CIA (amagat⁻²cm⁻¹)
0 - 40	4.16x10 ⁻⁸	3.21x10 ⁻⁸	2.16x10 ⁻⁸
40 - 100	1.67x10 ⁻⁷	1.48x10 ⁻⁷	1.16x10 ⁻⁷
100 - 160	2.39x10 ⁻⁷	2.46x10 ⁻⁷	2.34x10 ⁻⁷
160 - 220	2.60x10 ⁻⁷	2.97x10 ⁻⁷	3.23x10 ⁻⁷
220 - 280	4.29x10 ⁻⁷	4.59x10 ⁻⁷	4.73x10 ⁻⁷
280 - 330	1.12x10 ⁻⁶	9.48x10 ⁻⁷	7.82x10 ⁻⁷
330 - 380	2.22x10 ⁻⁶	1.64x10 ⁻⁶	1.19x10 ⁻⁶
380 - 440	2.20x10 ⁻⁶	1.81x10 ⁻⁶	1.51x10 ⁻⁶
440 - 495	1.90x10 ⁻⁶	1.62x10 ⁻⁶	1.51x10 ⁻⁶
495 - 545	2.93x10 ⁻⁶	3.91x10 ⁻⁶	3.15x10 ⁻⁶
545 - 617	6.14x10 ⁻⁶	5.84x10 ⁻⁶	4.97x10 ⁻⁶
617 - 667	5.77x10 ⁻⁶	5.71x10 ⁻⁶	5.11x10 ⁻⁶
667 - 720	3.61x10 ⁻⁶	3.97x10 ⁻⁶	4.13x10 ⁻⁶
720 - 800	2.11x10 ⁻⁶	2.63x10 ⁻⁶	3.24x10 ⁻⁶
800 - 875	1.40x10 ⁻⁶	1.93x10 ⁻⁶	2.68x10 ⁻⁶
875 - 940	8.83x10 ⁻⁷	1.30x10 ⁻⁶	2.10x10 ⁻⁶
940 - 1000	6.15x10 ⁻⁷	9.58x10 ⁻⁷	1.85x10 ⁻⁶

Table IIB: H₂-H₂ Collision-induced absorption values in the 1000 - 2050 cm⁻¹ spectral range.

	T = 150K	T = 200K	T = 300K
Wavenumber interval (cm⁻¹)	CIA (amagat⁻²cm⁻¹)	CIA (amagat⁻²cm⁻¹)	CIA (amagat⁻²cm⁻¹)
1000 - 1065	4.39x10 ⁻⁷	8.08x10 ⁻⁷	1.84x10 ⁻⁶
1065 - 1108	3.28x10 ⁻⁷	6.47x10 ⁻⁷	1.59x10 ⁻⁶
1108 - 1200	2.79x10 ⁻⁷	4.76x10 ⁻⁷	1.14x10 ⁻⁶
1200 - 1275	1.93x10 ⁻⁷	3.03x10 ⁻⁷	7.37x10 ⁻⁷
1275 - 1350	1.06x10 ⁻⁷	1.82x10 ⁻⁷	4.91x10 ⁻⁷
1350 - 1450	6.65x10 ⁻⁸	1.19x10 ⁻⁷	3.26x10 ⁻⁷
1450 - 1550	3.70x10 ⁻⁸	7.00x10 ⁻⁸	2.05x10 ⁻⁷
1550 - 1650	2.41x10 ⁻⁸	4.67x10 ⁻⁸	1.38x10 ⁻⁷
1650 - 1750	1.71x10 ⁻⁸	3.17x10 ⁻⁸	9.19x10 ⁻⁸
1750 - 1850	1.05x10 ⁻⁸	1.90x10 ⁻⁸	5.74x10 ⁻⁸
1850 - 1950	6.34x10 ⁻⁹	1.18x10 ⁻⁸	3.74x10 ⁻⁸
1950 - 2050	3.93x10 ⁻⁹	1.37x10 ⁻⁸	2.42x10 ⁻⁸

Table III: CO₂-CO₂ Collision-induced absorption values in the 0- 495cm⁻¹ and 1108-1850 cm⁻¹ spectral ranges.

	T = 150K	T = 200K	T = 300K
Wavenumber interval(cm⁻¹)	CIA (amagat⁻²cm⁻¹)	CIA (amagat⁻²cm⁻¹)	CIA (amagat⁻²cm⁻¹)
0 - 40	4.16x10 ⁻⁵	4.16x10 ⁻⁵	1.46x10 ⁻⁵
40 - 100	9.93x10 ⁻⁵	9.93x10 ⁻⁵	5.09x10 ⁻⁵
100 - 160	2.18x10 ⁻⁵	2.18x10 ⁻⁵	1.94x10 ⁻⁵
160 - 220	3.23x10 ⁻⁶	3.23x10 ⁻⁶	5.09x10 ⁻⁶
220 -280	4.26x10 ⁻⁷	4.26x10 ⁻⁷	1.20x10 ⁻⁶
280 - 330	6.36x10 ⁻⁸	6.36x10 ⁻⁸	3.06x10 ⁻⁷
330 - 380	1.1x10 ⁻⁸	1.1x10 ⁻⁸	8.63x10 ⁻⁸
380 - 440	1.57x10 ⁻⁹	1.57x10 ⁻⁹	2.11x10 ⁻⁸
440 - 495	2.04x10 ⁻¹⁰	2.04x10 ⁻¹⁰	4.80x10 ⁻⁹
1108 - 1200	3.14x10 ⁻⁷	2.94x10 ⁻⁷	2.93x10 ⁻⁷
1200 - 1275	7.91x10 ⁻⁶	6.48x10 ⁻⁶	5.8-x10 ⁻⁶
1275 - 1350	4.73x10 ⁻⁵	3.55x10 ⁻⁵	2.08x10 ⁻⁵
1350 - 1450	4.68x10 ⁻⁵	3.52x10 ⁻⁵	2.08x10 ⁻⁵
1450 - 1550	1.87x10 ⁻⁶	1.62x10 ⁻⁶	1.58x10 ⁻⁶
1550 - 1650	6.04x10 ⁻⁸	6.04x10 ⁻⁸	6.04x10 ⁻⁸
1650 - 1750	2.30x10 ⁻⁹	2.30x10 ⁻⁹	2.30x10 ⁻⁹
1750 - 1850	8.66x10 ⁻¹¹	8.66x10 ⁻¹¹	8.66x10 ⁻¹¹

Table IV: CH₄ radiative forcing for select atmospheres

fCO ₂	fH ₂	CH ₄ radiative forcing (W/m ²)
0.95	0	0.9
0.94	.05	1
0.79	0.20	0.43

REFERENCES

51. Kasting, J.F., Pollack, J.B., and D. Crisp. 1984. Effects of high CO₂ levels on surface temperature and atmospheric oxidation state of the early Earth. *J. Atmos. Chem.* 1, 403-428.
52. Pavlov A.A., Kasting, J.F., Brown, L.L., 2000. Greenhouse warming by CH₄ in the atmosphere of Early Earth. *J. Geophys. Res.* 105, E5, 11,981-11,990.
53. Haqq-Misra, J. D., Domagal-Goldman, S. D., Kasting, P. J. & Kasting, J. F. A revised, hazy methane greenhouse for the early Earth. *Astrobiol.* **8**, 1127-1137 (2008).
54. Kasting, J. F. CO₂ condensation and the climate of early Mars. *Icarus* **94**, 1-13 (1991).
55. Goldblatt C, Zahnle K., 2010. Clouds and the faint young Sun paradox. *Climate of the Past* 6: 1163-207.
56. Forget, F., Pierrehumbert, R.T., 1997. Warming early Mars with carbon dioxide clouds that scatter infrared radiation. *Science* 14, 1273-1276.
57. Mischna, M.A. Pavlov, A., Freedman, R., Kasting, J.F., 2000. Influence of carbon dioxide clouds on early Martian climate. *Icarus*, 145, 546-554.
58. Toon, O.B., McKay, C.P., Ackerman, T.P., Santhanam, K., 1989. Rapid calculation of radiative heating rates and photodissociation rates in inhomogeneous multiple scattering atmospheres. *J. Geophys. Res.*, 94, D13, 16,287 - 16,301.

59. Kopparapu, R., Ramirez, R., Kasting, J.F., Eymet, V., Robinson, T.D., Mahadevan, S., Terrien, R.C., Domagal-Goldman, S., Meadows, V., Deshpande, R., 2013. Habitable zones around main-sequence stars: new estimates. *Astrophysical Journal* 765.
60. Karkoschka, E., 1994. Spectrophotometry of the Jovian planets and Titan at 300 - 1000 nm wavelength: The methane spectrum. *Icarus*, 111, 1, 174-192.
61. Irwin, P.G.J., Calcutt, S.B., Taylor, F.W., Weir, A.L., 1996. Calculated k-distribution coefficients for hydrogen and self-broadened methane in the range 2000-9500 cm^{-1} from exponential sum fitting to band-modelled spectra. *J. Geophys. Res.* 101, 26,137-26,154.
62. Tian, F., M.W. Claire, J.D. Haqq-Misra, Smith, M., Crisp, D.C., Catling, D., Zahnle, K., Kasting, J.F., 2010. Photochemical and climate consequences of sulfur outgassing on early Mars. *Earth Planet. Sci. Lett.*, 295, 412-418.
63. Meadows, V.S., Crisp, D., 1996. Ground-based near-infrared observations of the Venus nightside: the thermal structure and water abundance near the surface. *J. Geophys. Res.*, 101, 4595-4622.
64. Wordsworth, R.D., Forget, F., Selsis, Eymet, V., 2010. Infrared collision-induced and far-line absorption in dense CO_2 atmospheres. *Icarus* 210, 992-997.
65. Perrin, M.Y., Hartmann, J.M., 1989. Temperature-dependent measurements and modeling of absorption by $\text{CO}_2\text{-N}_2$ mixtures in the far line-wings of the 4.3 micron CO_2 band. *JQRST*, 42, 4, 311-317.
66. Paynter, D.J., Ramaswamy, V., 2011. An assessment of recent water vapor continuum measurements upon longwave and shortwave radiative transfer. *J. Geophys. Res.* 116,D20302

67. Borysow, A., and L. Frommhold, 1986. Theoretical collision-induced rototranslational spectra for Modeling Titan's Atmosphere: H₂-N₂ Pairs. *Ap. J.*, 303, 495-510.
68. Burch, D.E., Gryvnak, R., Patty, R., Barky, C.E., 1969. Absorption of infrared radiant energy by CO₂ and H₂O. IV. Shapes of collision-broadened CO₂ lines. *J. Opt. Soc. Am.* 59, 3, 267- 280.
69. Kasting, J.F., 2013. How was early Earth kept warm? *Science* 339, 44.
70. Richard, C., Gordon, I.E., Rothman, L.S., Abel, M., Frommhold, L., Gustafsson, M., Hartmann, J.-M, Herman, C., Lafferty, W.J., Orton, G.S., Smith, K.M., Tran, H., 2012. New section of the HITRAN database: Collision-induced absorption (CIA). 113, 1276-1285.
71. Borysow, A., 2002. Collision-induced absorption coefficients of H₂ pairs at temperatures from 60K to 1000K. *A&A*, 390, 779 -782.
72. Halevy, I., Pierrehumbert, R.T., Schrag, D.P., 2009. Radiative transfer in CO₂-rich paleoatmospheres. *J. Geophys. Res.* 114, D18112, doi:10.1029/2009JD011915.
73. Gruszka, M., Borysow, A., 1997. Roto-Translational Collision-Induced Absorption of CO₂ for the atmosphere of Venus at frequencies from 0 to 250 cm⁻¹, at temperatures from 200 to 800K. *Icarus* 129, 172-177.
74. Gruszka, M., Borysow, A., 1998. Computer simulation of far-infrared collision induced absorption spectra of gaseous CO₂. *Molec. Phys.* 93, 6, 1007-1016.
75. Baranov, Y.I., Lafferty, W.J., Fraser, G.T., 2004. Infrared spectrum of the continuum and dimer absorption in the vicinity of O₂ vibrational fundamental in O₂/CO₂ mixtures. *Mol. Spectrosc.* 228, 432-440.

76. Brodbeck, C., Van-Thanh, N., Bouanich, J.-P., Boulet, C., Jean-Louis, A., 1991.
Measurements of pure CO₂ absorption at high densities near 2.3 μ m. J. Geophys. Res.
96, E2, 17,497-17,500.
77. de Bergh, C., Bezard, B., Crisp, D., Maillard, J.P., Owen, T., Pollack, J., Grinspoon,
D., 1995. Water in the deep atmosphere of Venus from high-resolution Spectra of the
night side. Adv. Space Res. 15, 4, (4)79-(4)88.
78. Pollack JB, Dalton, JB, Grinspoon, D, Wattson, R.B., Freedman, R., Crisp, D., Allen, D.A.,
Bezard, B., DeBergh, C., Giver, L.P., Ma, Q., Tipping, R. Near-infrared light from Venus'
nightside: A spectroscopic analysis. 1992. Icarus 103, 1-42.
79. Tsang, C.C.C., Irwin, P.G.J., Taylor, F.W., Wilson, C.F., 2008. A correlated-k model of
radiative transfer in the near-infrared windows of Venus. J. Quant. Spectrosc. Radiative
Transfer 109, 1118 - 1135.
80. Dalgarno, A., and Williams, D.A. ,1962. Rayleigh scattering by molecular hydrogen.
Ap.J.,136, 690-692.
81. Bucholtz, A., 1995. Rayleigh-scattering calculations for the terrestrial atmosphere.
Applied Optics. 34, 15, 2765-2773.
82. Edlen, B., 1966. The refractive index of air. Metrologia., 2, 71.
83. von Paris, P., Gebauer, S., Godolt, M., Grenfell, J.L., Hedelt, P., Kitzmann, D., Patzer,
A.B.C., Rauer, H., Stracke, B., 2010. The extrasolar planet Gliese 581d: A potentially
habitable planet? A&A 522, A23.
84. Chase, M.W., 1998. NIST-JANAF thermochemical tables. American Chemical Society, 9,
4th edition, 1951 pp.

85. Kasting, J. F., Brown, L. L. 1998. Setting the stage: the early atmosphere as a source of biogenic compounds. In *The Molecular Origins of Life: Assembling the Pieces of the Puzzle*, ed. A. Brack, pp. 35-56. New York: Cambridge Univ. Press
86. Kasting, J. F., Canfield, D. E. 2012. The global oxygen cycle. In *Fundamentals of Geobiology*, ed. KO Konhauser, AH Knoll, D Canfield, pp. 93-104. Oxford: Wiley-Blackwell
87. Pavlov AA, Kasting JF, Brown LL. 2001. UV-shielding of NH₃ and O₂ by organic hazes in the Archean atmosphere. *J. Geophys. Res.* 106: 23,267-23,87
88. Pinto JP, Gladstone CR, Yung YL. 1980. Photochemical production of formaldehyde in the earth's primitive atmosphere. *Science* 210: 183-185
89. Jarrard, R. D. Subduction fluxes of water, carbon dioxide, chlorine, and potassium. *Geochemistry Geophysics Geosystems* **4** (2003).
90. Wetzel, D. T., Rutherford, M. J., Jacobsen, S. D., Hauri, E. H., and Saal, A. E. 2013. Degassing of reduced carbon from planetary basalts. *Proceedings of the National Academy of Sciences of the United States of America* **110**, 8010-8013.
91. Forget, F. *et al.*, 2013. 3D modelling of the early martian climate under a denser CO₂ atmosphere: Temperatures and CO₂ ice clouds. *Icarus* **222**, 81-99.
92. Kitzmann, D., Patzer, A.B.C., Rauer, H., 2013. Clouds in the atmospheres of extrasolar planets. *A&A*, in press.